Chem Soc Rev

Thermopower measurements in molecular junctions

Chem Soc Rev

REVIEW ARTICLE

Thermopower measurements in molecular junctions

Laura Rincón-García[ab], Charalambos Evangeli[a], Gabino Rubio-Bollinger[ac] and Nicolás Agraït*[abc]

The measurement of thermopower in molecular junctions offers complementary information to conductance measurements and is becoming essential for the understanding of transport processes at the nanoscale. In this review, we discuss the recent advances in the study of the thermoelectric properties of molecular junctions. After presenting the theoretical background for thermoelectricity at the nanoscale, we review the experimental techniques for measuring the thermopower in these systems and discuss the main results. Finally, we consider the challenges in the application of molecular junctions in viable thermoelectric devices.

1. Introduction

The idea of using molecules as electronic components in functional devices has impelled an extensive experimental and theoretical research of charge transport through molecular junctions, that is, single molecules connected between two metallic electrodes.[1] Some basic electronic functions have been demonstrated,[2] but, more importantly, molecular junctions have proved to be an exceptional platform to test quantum transport theories and have greatly contributed to our understanding of charge transport at the nanoscale. While most studies have focused on the conductance of the junction, recently the possibility of measuring other important properties like mechanical, optical, magnetic, or thermal has been explored.[2,3] In this review, we will focus on the thermoelectric properties of molecular junctions, which arise from the coupling between thermal transport and charge transport.

Similarly to what occurs in a bulk material, when the two sides of a molecular junction are at different temperatures, T_1 and T_2, a voltage difference, $V_1 - V_2$, proportional to the temperature difference, appears (see Fig. 1). This is normally written as

$$V_1 - V_2 = -S(T_1 - T_2), \qquad (1)$$

where S is the *thermopower* or *Seebeck coefficient*. Why is it interesting to measure the thermopower of a molecular

junction in addition to its conductance? There are two reasons. Firstly, the measurement of the thermopower gives an additional fundamental insight into the electronic structure of the junction and its transport properties.[4] Secondly, and most importantly, the study of molecular junctions might pave the way to the development of new environmentally-friendly organic-based thermoelectric devices with a lower cost than present inorganic semiconducting thermoelectrics. Devices with a high thermoelectric efficiency would enable direct conversion of heat into electricity in energy harvesting applications or on-chip cooling in nanoscale electronic devices. Molecular junctions are promising candidates to achieve these high efficiencies due to the discreteness of the energy levels responsible for transport and the tunability of their properties via chemical synthesis, electrostatic gates, or pressure.

In this review, we will give an overview of the methods used to measure the thermopower in molecular junctions and examine the main results reported. We must note that the investigation of thermoelectricity in bulk organic materials, which constitutes a separate topic, will not be reviewed. In Section 2, we will provide the theoretical background for quantum transport through a molecular junction when both a voltage gradient and a temperature gradient are present. We will also discuss the difference between thermopower at the nanoscale (quantum thermopower) and bulk thermopower, and the transition from bulk to nano. The last part of this

a. *Departamento de Física de la Materia Condensada and Condensed Matter Physics Center (IFIMAC), Universidad Autónoma de Madrid, E-28049 Madrid, Spain. E-mail: nicolas.agrait@uam.es*
b. *Instituto Madrileño de Estudios Avanzados en Nanociencia IMDEA-Nanociencia, E-28049 Madrid, Spain*
c. *Instituto Universitario de Ciencia de Materiales "Nicolás Cabrera", Universidad Autónoma de Madrid, E-28049 Madrid, Spain*
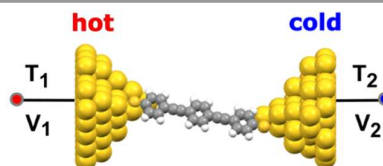
Fig. 1 Thermovoltage measurement in a molecular junction. When the two sides of a molecular junction are at different temperatures, T_1 and T_2, a voltage difference, $V_1 - V_2 = -S(T_1 - T_2)$, where S is the Seebeck coefficient of the molecular junction, appears between the two electrodes.

section will be dedicated to the efficiency of thermoelectric devices, an essential topic for thermoelectric applications. We will then review, in Section 3, the experimental methods currently used to measure the thermopower in molecular junctions and review the main results reported. Section 4 is devoted to thermopower measurements in metallic contacts, which give valuable complementary information about thermoelectricity at the nanoscale. Finally, in Section 5, the current challenges and future perspectives in the field of molecular junction thermoelectricity will be discussed.

2. Theoretical background

Molecular junctions are atomic-scale systems, hence much smaller than the electron mean free path in the electrodes. As a consequence, in order to describe transport, a full quantum approach is required in contrast to bulk systems, which can be described using a semiclassical approach. In this section, we will first introduce the general theoretical background needed to understand thermoelectricity in molecular junctions and then discuss the differences and similarities between nanoscale and bulk thermopower. We will finish this section examining the concept of thermoelectric efficiency. We refer the interested reader to the excellent book by J.C. Cuevas and E. Scheer[1] and the review paper by Y. Dubi and M. di Ventra[5] for more details.

2.1 Quantum conductance and thermopower

The electrical current through a nanoscale object and, in particular, through a molecular junction, depends on the transmission probability for an electron to cross through the junction from the left-hand side electrode to the right-hand side electrode. The *transmission* of the junction is a function of the electron energy and depends on the electronic structure of the molecule (its molecular orbitals), which is modified by the coupling to the contacts. Thus, in the case of non-interacting charge carriers, the transmission is correctly described by Landauer's formula and the current through the junction I is then given by

$$I = \frac{2e}{h} \int_0^\infty d\varepsilon \, \mathcal{T}(\varepsilon)[f_L(\varepsilon) - f_R(\varepsilon)], \qquad (2)$$

where $\mathcal{T}(\varepsilon)$ is the transmission probability of an electron at energy ε, e is the electron's charge, h is Planck's constant and f_L and f_R are the Fermi distributions of the left and right leads, respectively, given by $f_i = \left(1 + e^{(\varepsilon - \mu_i)/k_B T}\right)^{-1}$, $i = L, R$; where μ_i is the chemical potential of the corresponding electrode, k_B is the Boltzmann constant and T is the temperature. The difference of the left and right distribution functions depends on the temperature ΔT and chemical potential difference $\Delta \mu$ between the leads:

$$f_L(\varepsilon) - f_R(\varepsilon) = -\frac{\partial f}{\partial \varepsilon} \Delta \mu - \frac{\partial f}{\partial \varepsilon}\left(\frac{\varepsilon - \mu}{T}\right)\Delta T. \qquad (3)$$

Introducing eqn (3) in eqn (2) and taking into account that the difference of the chemical potentials is set by the voltage

difference between the two leads $\Delta V = \Delta \mu / e = (\mu_L - \mu_R)/e$, the current can be expressed as

$$I = G\Delta V + L_T \Delta T = G\Delta V + GS\Delta T, \qquad (4)$$

where the *conductance* G and $L_T = GS$ are given by

$$G = \frac{2e^2}{h} \int_0^\infty d\varepsilon \, \mathcal{T}(\varepsilon)\left(-\frac{\partial f}{\partial \varepsilon}\right), \qquad (5)$$

$$L_T = GS = \frac{2e}{h}\frac{1}{T} \int_0^\infty d\varepsilon \, \mathcal{T}(\varepsilon)\,(\varepsilon - \mu)\left(-\frac{\partial f}{\partial \varepsilon}\right), \qquad (6)$$

where S is the thermopower or Seebeck coefficient. Eqn (4) shows that the electrical current through the junction is the sum of a bias-induced current and a temperature-induced current. In open circuit, the current will be zero and a *thermovoltage* V_{th} appears between the two electrodes

$$V_{th} = -\frac{L_T}{G}\Delta T = -S\Delta T. \qquad (7)$$

Note that this is also the voltage difference that is necessary to apply to cancel the current and that ΔT is the temperature difference between the leads (one electron mean free path away from the junction). From eqn (4) we can see that for zero applied bias, a *thermocurrent* I_{th} will flow due to the temperature difference between the two electrodes,

$$I_{th} = GS\Delta T. \qquad (8)$$

Explicitly, the thermopower is given by

$$S(T) = -\frac{1}{e\,T}\frac{\int_0^\infty d\varepsilon \, \mathcal{T}(\varepsilon)(\varepsilon - \mu)\left(-\frac{\partial f}{\partial \varepsilon}\right)}{\int_0^\infty d\varepsilon \, \mathcal{T}(\varepsilon)\left(-\frac{\partial f}{\partial \varepsilon}\right)}. \qquad (9)$$

In the low temperature limit and assuming that there are no transmission resonances close to the equilibrium chemical potential, we can simplify the expressions for the conductance and the thermopower to

$$G = \frac{2e^2}{h}\mathcal{T}(\varepsilon_F) = G_0 \mathcal{T}(\varepsilon_F), \qquad (10)$$

$$S(T) = -\frac{\pi^2}{3}\frac{k_B^2 T}{e}\frac{1}{\mathcal{T}(\varepsilon_F)}\frac{d\mathcal{T}(\varepsilon)}{d\varepsilon}\bigg|_{\varepsilon_F} = -\frac{\pi^2}{3}\frac{k_B^2 T}{e}\frac{\mathcal{T}'(\varepsilon_F)}{\mathcal{T}(\varepsilon_F)}, \qquad (11)$$

where ε_F is the Fermi level and G_0 is the *quantum of conductance*. Eqn (11) shows that the thermopower depends on the variation of the transmission for carriers above and below the Fermi level: larger transmission above Fermi level will cause the electrons to go to the cold electrode resulting in negative thermopower and the conversely, as illustrated in Fig. 2 for a molecular junction. It must be remarked that these
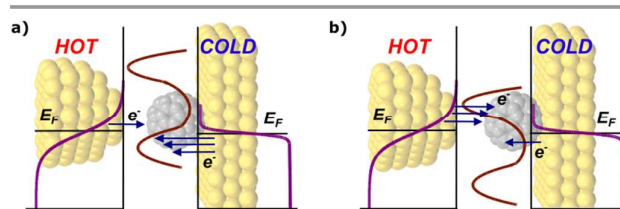

Fig. 2 Sign of the thermopower. (a) Electrons below the Fermi level have larger transmission probability than those above: the net flow of electrons will be to the hot side and $S > 0$. (b) Electrons above the Fermi level have larger transmission probability than those below: the net flow of electrons will be towards the cold side and $S < 0$.

equations are only valid for non-interacting charge carriers, since they are based on Landauer formalism, and they also ignore the interaction between phonons and electrons, *i.e.*, phonon drag (see ref. 5 for a full discussion of their validity).

Thermopower, in contrast with conductance, is an intensive property and is independent of the number of molecules participating in a molecular junction. This can be understood by considering N identical molecules in parallel in a junction. Assuming that interference effects are negligible, the total transmission of the junction will be $\mathcal{T}_N = N\mathcal{T}_1$, where $\mathcal{T}_1$ is the transmission of one molecule, and applying eqn (11) we obtain that the thermopower of the junction $S_N = S_1$, where S_1 is the thermopower of a single molecule.

As we have seen above, for calculating the thermopower of a molecular junction in Landauer's approach, we must simply obtain the transmission $\mathcal{T}(\varepsilon)$. This is normally done by calculating the electronic structure using density functional theory (DFT) and computing the transmission function with the help of Green's function techniques.[6,7] In addition to the lack of exact knowledge of the geometry of the junction, which has a strong impact on the transmission, the results obtained from DFT calculations present many theoretical uncertainties and cannot be considered exact. In this respect, comparison of the theory with the experimental values of both conductance and thermopower, which are given by the transmission and its slope at the Fermi level, respectively, enables to gain insight into the relative energy alignment and provides an essential feedback to obtain a more accurate description of the molecular junction.

We will now consider a simple model (the so-called *two level model*), that only takes into account the frontier orbitals of the molecule and allows to gain some basic understanding of the important aspects of the thermopower of molecular junctions. Denoting the positions of the highest occupied molecular orbital (HOMO) and the lowest unoccupied molecular orbital (LUMO) by ε_1 and ε_2, respectively, we may

approximate the transmission as the sum of two Breit-Wigner resonances,[1,4]

$$\mathcal{T}(\varepsilon) = \sum_{i=1}^{2} \frac{4\Gamma_{iL}\Gamma_{iR}}{(\varepsilon-\varepsilon_i)^2+(\Gamma_{iL}+\Gamma_{iR})^2} \,, \qquad (12)$$

where Γ_{1L}, Γ_{2L} and Γ_{1R}, Γ_{2R}, represent the coupling to the left and right electrodes of the HOMO and LUMO, respectively (see Fig. 3). The conductance and thermopower depend on the value of this function and its derivative at $\varepsilon = \varepsilon_F$ (eqn (10) and (11)) and, consequently, the position of the HOMO and LUMO with respect to the Fermi level of the electrodes, the so-called *level alignment,* is crucial in determining the transport properties of the junction. Thus, S will be positive if the Fermi level is closer to the HOMO and negative if it is closer to the LUMO, and most importantly, S will have a larger magnitude in the proximity of the resonances where the slope of the transmission will be larger. Tuning the level alignment with the goal of maximizing the thermopower is one of the key strategies in the experimental research on the thermoelectric properties of molecular junctions. In the case of HOMO-dominated transport, since $S > 0$, one may speak of hole-like carriers, whereas for LUMO-dominated transport, $S < 0$ and the carriers are considered electron-like (*cf.* Fig. 2).

We can also draw an important conclusion from Fig. 3 observing how the transmission resonances vary with the coupling of the molecule to the electrodes. Clearly, a smaller coupling results in steeper HOMO and LUMO resonances and hence, in a larger thermopower, although conductance is lower.

Another potentially important effect on the thermopower of molecular junctions is quantum interference in the form of Fano resonances[8] or transmission nodes.[9] In the case of the Fano resonance, the interference effect originates when a molecule in a molecular junction has a side group not connected to the electrodes. The transmission close to one of the molecular resonances will not be just a Breit-Wigner resonance, but will have the form
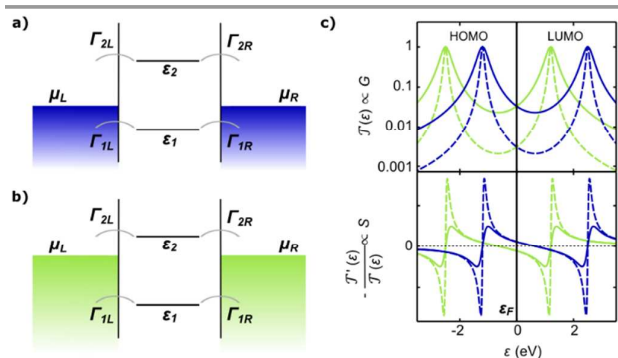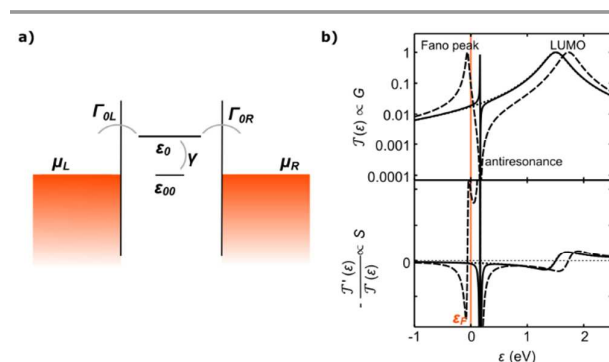

Fig. 3 Two level model. (a,b) Energy diagram for the molecular junction in the absence of a voltage bias ($\mu_L = \mu_R$, where $\mu_{L,R}$ is the chemical potential of the left and right electrodes, respectively). Two different alignments are presented: in (a) the Fermi level is closer to the HOMO and in (b) it is closer to the LUMO. (c) $\mathcal{T}(\varepsilon)$ and $-\mathcal{T}'(\varepsilon)/\mathcal{T}(\varepsilon)$ for the two level model described by eqn (12). The blue curves correspond to (a) $\varepsilon_1 = -1.2$ eV and $\varepsilon_2 = 2.5$ eV, and the green ones to (b) $\varepsilon_1 = -2.5$ eV and $\varepsilon_2 = 1.2$ eV. The thermopower is proportional to $-\mathcal{T}'(\varepsilon)/\mathcal{T}(\varepsilon)$ at the Fermi level ε_F, and hence positive for (a) and negative for (b). Two different couplings of the molecules to the electrodes have been considered: $\Gamma_{iL} = \Gamma_{iR} = 0.1$ eV (solid line) and $\Gamma_{iL} = \Gamma_{iR} = 0.03$ eV (dashed line), weaker coupling, where $i = L, R$. After ref. 1.

Fig. 4 Fano resonance in the transmission function. (a,b) Energy diagram (a) and $\mathcal{T}(\varepsilon)$ and $-\mathcal{T}'(\varepsilon)/\mathcal{T}(\varepsilon)$ (b) for a molecular junction in the case of a Fano resonance present close to the LUMO, and in the absence of voltage bias ($\mu_L = \mu_R$, where $\mu_{L,R}$ are the chemical potential of the left and right electrodes, respectively). $\mathcal{T}(\varepsilon)$ and $-\mathcal{T}'(\varepsilon)/\mathcal{T}(\varepsilon)$ are calculated from the model described by eqn (13), using $\varepsilon_0 = 1.5$ eV, $\varepsilon_{00} = 0.17$ eV (resonance close to the LUMO) and $\Gamma_{0L} = \Gamma_{0R} = 0.1$ eV, and considering three different resonant couplings: $\gamma = 0$ eV (dotted line), $\gamma = 0.1$ eV (solid line), and $\gamma = 0.6$ eV (dashed line). If the Fano peak is at the Fermi level, it will have a large impact on both the conductance and the thermopower. After ref. 1.
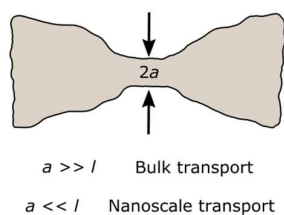
Fig. 5 Bulk *vs.* nanoscale transport. In a constriction between two conductors, the ratio of the constriction radius a to the electron mean free path l determines the transport regime: if $a \gg l$, the charge carriers would drift through the constriction when a voltage or temperature gradient is applied, while for $a \ll l$, they would move ballistically. Note that, in a constriction, the voltage or temperature will drop in a distance of the order of the constriction diameter.

$$\mathcal{T}(\varepsilon) = \frac{4\Gamma_{0L}\Gamma_{0R}}{[\varepsilon-\varepsilon_0-\gamma^2/(\varepsilon-\varepsilon_{00})]^2+(\Gamma_{0L}+\Gamma_{0R})^2}, \quad (13)$$

where Γ_{0L} and Γ_{0R} represent the coupling to the electrodes; ε_0 and ε_{00} are the position of the molecular level and of the side level, respectively; and γ is the coupling of the molecular level and the side level (see Fig. 4). When the side group is weakly coupled to the backbone, that is, $\gamma \ll |\varepsilon_0 - \varepsilon_{00}|$, the transmission has a Breit-Wigner resonance at $\varepsilon = \varepsilon_0$ and an antiresonance at $\varepsilon = \varepsilon_{00}$, where the transmission vanishes. In addition, it has a Fano peak at $\varepsilon \cong \varepsilon_{00} - \gamma^2/|\varepsilon_0 - \varepsilon_{00}|$. If the Fano peak is at the Fermi level, it will have a large impact on the conductance and the thermopower. An in-depth tutorial review on quantum interference effects can be found in ref. 10.

2.2 Nanoscale thermopower *vs*. bulk thermopower

The thermopower at the nanoscale is correctly described by eqn (11), which is similar to Mott's semiclassical formula for bulk materials,[11]

$$S(T) = -\frac{\pi^2}{3}\frac{k_B^2 T}{e}\frac{\sigma'(\varepsilon_F)}{\sigma(\varepsilon_F)}, \quad (14)$$

where σ is the electrical conductivity. However, it is important to remark that this similarity is misleading, because the physical mechanisms that determine the thermopower are different. For instance, in a metal at ambient temperature, the thermopower is dominated by electron diffusion, since above the Debye temperature the phonon drag contribution is negligible. The sign and magnitude of $\sigma'(\varepsilon_F)/\sigma(\varepsilon_F)$, and consequently of the thermopower, depend on the energy dependence of the conductivity around the Fermi energy, which in turn depends on the inelastic relaxation time and the effective mass. In contrast, at the nanoscale, the term $\mathcal{T}'(\varepsilon_F)/\mathcal{T}(\varepsilon_F)$ depends on the geometry of the nanoconstriction and local electronic structure. Evangeli *et al.*[12] have recently studied the transition between the two regimes, finding that it is determined by the ratio of the constriction size to the electron mean free path. This is illustrated in Fig. 5 (see more details in Section 4).

In Table 1, we have compiled in the thermopower of different bulk materials to illustrate typical values. Metals normally have small thermopower value (of the order of

Table 1 Thermopower values at room temperature for several metals, semiconductors, and organic polymers. Metals' Seebeck coefficient is normally small (of the order of $\pm 1 - 10$ μV K^{-1}), while semiconductors' is much higher ($\pm 100 - 1000$ μV K^{-1}).

Material	Thermopower S (μV K^{-1})
Metals	
Au	1.94^a
Ag	1.51^a
Cu	1.83^a
W	1.07^a
Pt	-5.28^a
Ni	-19.5^b
Al	-1.66^b
Pb	-1.05^b
Bi	$\sim -50^c$
Bi nanowire	$\sim -75^d$
Semiconductors	
Si	450^b // -86^e
Ge p-type	$\sim 920^f$
Ge n-type	$\sim -1100^f$
SiGe p-type bulk	$\sim 170^g$
SiGe n-type bulk	$\sim -180^h$
PbSe p-type bulk	$\sim 375^i$
Bi$_2$Te$_3$ p-type bulk	$\sim 210^b$
Bi$_2$Te$_3$ n-type bulk	$\sim -250^b$
Bi$_2$Te$_2$Se thin films	-200^j
Si nanowire	240^k
Organic polymers	
PEDOT:PSS (thin film)	$\sim 73^l$
PEDOT:PSS (thick film)	161^m

^{a} Ref. 13. ^{b} Ref. 14. ^{c} Ref. 15. ^{d} Ref. 16. ^{e} Ref. 17. ^{f} Ref. 18. ^{g} Ref. 19. ^{h} Ref. 20. ^{i} Ref. 21. ^{j} Ref. 22. ^{k} Ref. 23. ^{l} Ref. 24. ^{m} Ref. 25.

$\pm 1 - 10$ μV K^{-1}), while semiconductors can be n-doped (negative carriers) or p-doped (positive carriers) to much higher values of the thermopower ($\pm 100 - 1000$ μV K^{-1}).

2.3 Thermoelectric efficiency: the figure of merit *ZT*

If we want to think in applications of molecular junctions, we have to consider the efficiency of a thermoelectric device or a material for converting thermal to electrical energy or for refrigeration. This efficiency depends on the dimensionless *figure of merit*,[26] which in the case of a bulk material is given by:

$$ZT = \frac{\sigma S^2 T}{\kappa}, \quad (15)$$

where σ and κ are the electrical and thermal conductivity, respectively. In a conducting material heat is transported by electrons and phonons and, consequently, $\kappa = \kappa_{el} + \kappa_{ph}$. Note that ZT only depends on the physical properties of the material and not on the geometry. In contrast, for molecular junctions, the figure of merit is

$$ZT = \frac{GS^2 T}{K}, \quad (16)$$

where G is the electrical conductance and $K = K_{el} + K_{ph}$ is the thermal conductance of the molecular junction, which

again can be decomposed into electron and phonon contributions. Note that measuring experimentally the figure of merit of a molecular junction requires, in addition to measuring the thermopower and electrical conductance, the thermal conductance, which is a very demanding task due to the minute thermal flows involved. Up to date, no experimental measurement of the thermal conductance in single-molecule junctions has been reported.

We can obtain a lower bound on acceptable values of S for efficient molecular junctions. Writing explicitly the electron and phonon contributions to the thermal conductance, we have

$$ZT = \frac{GS^2T}{K_{el}+K_{ph}} = \frac{GS^2T}{K_{el}\left(1+K_{ph}/K_{el}\right)} = \frac{S^2}{L_0\left(1+K_{ph}/K_{el}\right)} \qquad (17)$$

where we have taken into account that the ratio of thermal conductance due to the electrons to the electrical conductance is proportional to the temperature $L_0T = K_{el}/G$, where L_0 is the Lorenz number. The most favourable case is when all the heat is carried by the electrons (phonon contribution is negligible) as in the case of metals at ambient temperatures. Taking into account that for practical applications $ZT > 1$, we find that $S > 150\ \mu V\ K^{-1}$. Note that when the contribution of the phonons to the thermal conductance becomes important, a high efficiency would require higher thermopower.

Quantum interference effects in a molecular junction would have an important impact on the figure of merit. As we saw before, a resonance at the Fermi energy has a large effect on S and G, but should have a negligible effect on the thermal conductance due to phonons, leading to a significant enhancement of ZT.[10,27-29]

3. Experimental measurements of the thermopower of molecular junctions

The experimental techniques used to measure the thermoelectric properties of molecular junctions derive from those developed to measure their conductance. In most cases, they aim at probing just a single molecule connected between two metal electrodes and employ scanning tunnelling microscope (STM) based techniques,[30-32] mechanically controlled break junctions (MCBJ),[33,34] or electromigrated break junctions.[35] In other experiments, small area molecular junctions consisting of self-assembled monolayers (SAMs) on a conducting substrate contacted with a conducting-probe atomic force microscope (CP-AFM),[36] or even networks of molecular junctions in nanoparticle arrays[37] have been investigated. In all the cases, measurements require the connection of the molecule to two electrodes, whose separation cannot be larger than the length of the molecule, typically $1-3$ nm.

These techniques can be divided in two broad groups regarding to how the junctions are formed. In *dynamic* techniques, like the break junction technique and AFM-based techniques, the junction is formed during the experiment and the evolution of the junction gives relevant information about its structure. In *static* techniques, the molecular junctions are fabricated and then their transport properties are measured, suffering no modification during that measurement. This is the case of electromigrated break junctions and nanoparticle arrays.

Measuring the thermopower of molecular junctions requires, besides the junction formation itself, establishing a well-defined temperature difference between the two sides of the junction. For STM-based techniques, this is quite straightforward; since the tip is connected to a large thermal reservoir and the thermal conductivity of the tip (typically Au) is large compared to the junction, the tip apex will be practically at the same temperature as the reservoir.[30] Either the tip or the substrate can be resistively or thermoelectrically (*i.e.*, using a Peltier element) heated. In contrast, in other techniques, like electromigrated break junctions, establishing the temperature gradient can be a major challenge. In addition, it is essential to consider the thermal circuit (see below in section 3.2) and take into consideration all temperature drops, since temperature gradients give rise to thermovoltages in all conducting materials, to correctly determine the thermovoltage at the junction.

Now we will describe the different techniques that are used to measure the thermoelectric properties of molecular junctions, appraising their strengths and weaknesses and giving an account of the most relevant results obtained.

3.1 Break junction technique: fabrication of a molecular junction

The simplest and most widely used method to measure the properties of molecular junctions is the break junction technique, based on the techniques developed to study metallic atomic contacts.[38-41] In this dynamic technique, which can be implemented using a STM (STM-BJ technique) or a MCBJ, the measurement is carried out as the junction is formed. The starting point of the experiment is a contact between two metallic electrodes, *i.e.*, the two sides of a MCBJ or the tip and sample in the case of a STM-BJ (see Fig. 6a), which can be regarded as a metallic constriction between two bulk electrodes. When the two electrodes are pulled apart in a controlled way, the constriction deforms plastically, decreasing in diameter as its length increases and, as a consequence, the conductance of the contact decreases.

The conductance traces during breaking exhibit features characteristic of the composition of the electrodes.[42] In the case of gold, which is the most commonly used electrode material, the conductance decreases stepwise presenting a clear plateau at $G = G_0 = 2e^2/h$, the quantum of conductance, just before the final rupture (see Fig. 6). At this point, the contact consists of a single gold atom with a single totally open conductance channel. Further pulling breaks this one-atom contact and the conductance decreases exponentially as the electrodes separate entering the tunnelling regime. Atomic-sized metallic contacts of many different metals have been investigated.[41] It was found that each metal presents a characteristic breaking pattern in the conductance traces and that, in most metals, the conductance of a one-atom contact is differs from G_0 due to the presence of partially open quantum channels.[43] We must note that, for gold and platinum, at cryogenic temperatures, atomic chains may form with a low probability,[44,45] but these chains are never observed in ambient conditions. Additionally, the forces needed to break an atomic contact of gold have been measured at low[45,46] and ambient[47] temperatures.

Now, if the metallic contact is broken in the presence of molecules, as first reported by Reed *et al.*[48] for MCBJ and Xu *et al.*[49] for STM-BJ, one of these molecules can be trapped between the tip and the substrate showing as a plateau in the conductance at a value lower (typically orders of magnitude) than 1 G_0 (see Fig. 7). In general, the molecules under study are provided with adequate linker groups at both ends to facilitate binding to the electrodes, and it is considered important to form first a metallic contact in order to ensure that there is a reduced number of molecules in the contact area and to have a reference for the separation of the electrodes.
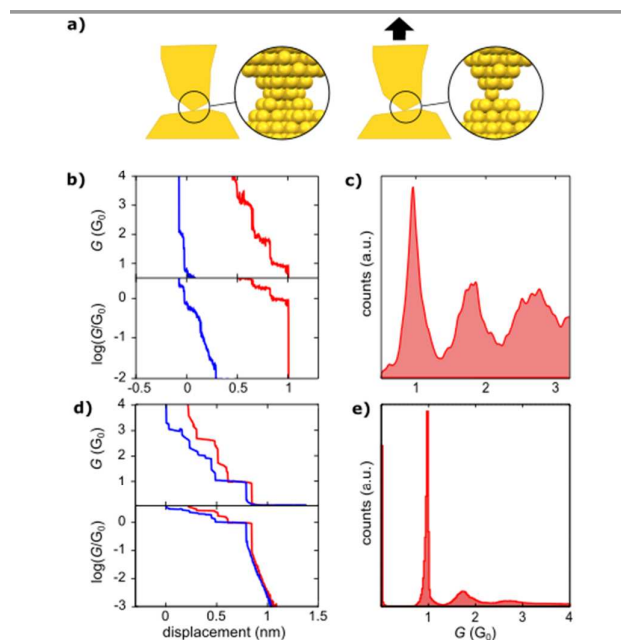

Fig. 6 Metallic atomic contacts. (a) Schematic representation of atomic contact formation. (b) Conductance evolution during contact formation (blue curve) and contact breaking (red curve) for Au atomic contacts, in linear (top panel) and logarithmic scale (bottom panel) at room temperature in ambient conditions using a STM. (c) Conductance histogram for 1591 contact breakings. (d,e) The same as for (b) and (c), respectively, but at low temperatures (4.2 K). In (e), the conductance histogram contains around 6000 contact breakings.
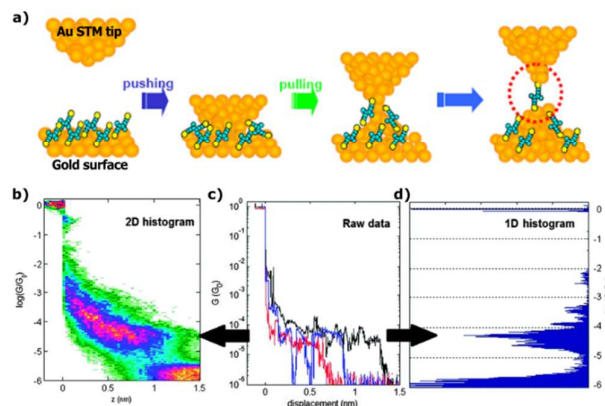
Fig. 7 Break junction technique. (a) Schematic representation of STM-BJ technique. Breaking of the gold atomic contact typically results in the formation of a protrusion on the substrate due to plastic deformation.[44] (c) Examples of individual conductance *G vs.* electrode displacement traces where the plateau indicates the formation of a molecular junction. (b,d) Conductance histogram (d) and 2d-histogram of conductance *G vs.* electrode displacement (b) generated out of individual conductance traces. Adapted from ref. 50 with permission from The Royal Society of Chemistry.

These low conductance plateaus in the conductance traces are ascribed to one molecule bridging the gap between the electrodes, however the possibility of having more than one molecule in close proximity cannot be ruled out. In addition, the large dispersion observed in the plateau values is likely to be due to the various possible binding configurations of the molecule in the junction. This makes convenient to gather the results of many breaking traces in a conductance histogram, which presents peaks at the conductance of the most probable configurations, and that is normally considered to be the conductance of a single-molecule junction. A 2d-histogram of the conductance traces *vs.* tip displacement also gives valuable information about the breaking length, which is related to the length of the molecule (see Fig. 7).[50]

The break junction technique is the most used due to its relative simplicity and versatility. Experiments can be performed in solution and in ambient conditions (using gold electrodes). The main drawback of the technique is the lack of precise knowledge of the number of molecules participating in the junction and their configuration.

3.2 Break junction technique: thermopower measurements

The Seebeck coefficient can be determined by performing either a *voltage* measurement or a *current* measurement (see Fig. 8). In the first approach, a voltage amplifier is used to measure the voltage across the junction (thermovoltage) in an open circuit configuration and eqn (7) is used to get S. In the second approach, the current at zero applied bias (thermocurrent) is measured with the help of a current amplifier, or alternatively, the voltage necessary to suppress the current is determined. Eqn (8) is then used to obtain S. Both approaches are equivalent but, as we will show below,
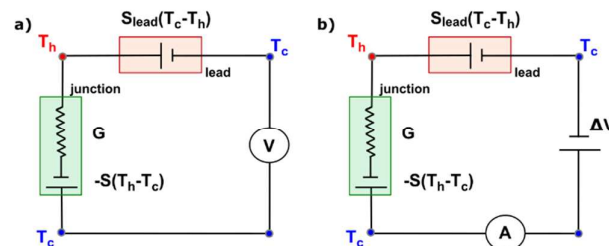

Fig. 8 Electrical circuit and equivalent thermal circuits to be considered for measuring the Seebeck coefficient of molecular junctions. (a) Voltage measurement in open circuit (thermovoltage). (b) Current measurement when a voltage difference ΔV is applied. In both approaches, one side of the junction is at temperature T_c and the other at $T_h = T_c + \Delta T$. Hence the junction (marked in green) is electrically equivalent to a conductance G and a thermovoltage. It is also essential to consider the thermovoltage that appears in the connecting lead (marked in red) due to the temperature gradient. S and S_{lead} are the thermopower of the junction and the conducting parts of the circuit, respectively.

the current measurement approach is more advantageous for STM-based setups, because in this case the current is used to monitor the junction formation and, consequently, no switching to a voltage measurement circuit is required.

3.2.1 Voltage measurement technique. The first measurement of the thermopower of a molecular junction was reported in 2007 by the group of R. A. Segalman.[30] The measurement was performed in ambient conditions using the break junction technique in a modified STM. A temperature difference ΔT between the Au tip and the Au substrate is established by heating the substrate resistively and maintaining the tip temperature very close to ambient. The modified microscope can be switched between two modes: a *current* mode, which is the standard STM-BJ mode, in which a current amplifier is used to record the tip-substrate current under a bias voltage, and a *voltage* mode where a voltage amplifier records the thermoelectric voltage induced between tip and substrate (see Fig. 9a). The measurement is performed in two distinct phases: the STM tip approaches the substrate in the current mode and, when the conductance reaches a preset current threshold indicating the formation of a molecular junction, the STM is switched to the voltage mode and the tip is slowly retracted. The resulting thermovoltage *vs.* tip displacement curve shows a rather constant value until the junction breaks, which is signalled by a sudden voltage drop (see Fig. 9b). The values obtained from many different measurements are collected in a thermovoltage histogram whose mean value is the thermovoltage of the molecular junction. In general, measurements of the thermovoltage are performed at ambient conditions at about 300 K and using various temperature gradients up to $\Delta T = 40$ K (as shown in Fig. 9c). The position of the thermovoltage peak shows a linear dependence on ΔT from which the value of the thermopower S is extracted (see Fig. 9d).[51]

The main drawback of this technique is that thermopower and conductance cannot be measured simultaneously and, consequently, the evolution of the junction during breaking is not known.

3.2.2 Thermoelectric current measurement technique. In order to avoid switching between the standard STM current amplifier to a voltage amplifier, one can obtain the thermopower of the junction from a current measurement. The group of L. Venkataraman reported such a method in 2012 (see Fig. 10).[31] The measurement starts by bringing the tip in contact with the substrate under a given voltage bias until a conductance larger than G_0 is reached ($\sim 5G_0$). Then it is withdrawn to a preset distance, which depends on the length of the molecule being probed, and the bias voltage is set to zero for a short time interval. The voltage bias is re-established and the tip is further retracted. The measurement of the current while the tip is stationary yields the conductance and thermocurrent and hence the thermopower (using eqn (8)) of a given molecular junction. The main advantage of this technique over the voltage measurement technique described in the previous subsection is that conductance and thermopower are measured in the same junction.

The previously described techniques to measure the thermopower share the drawback that the evolution of conductance and thermopower cannot be followed simultaneously. This is an important question in molecular junctions because the evolution of the conductance during junction formation gives essential information about its structure. A powerful technique, also based in the measurement of current, that overcomes this issue by measuring simultaneously the conductance and thermopower during the whole evolution of the molecular junctions, was developed by the group of N. Agraït in 2013.[32] In this case, the motion of the STM tip during approach and retraction is halted at short intervals during a few milliseconds and the voltage is ramped to acquire IV curves. The slope of these IV curves is the conductance G and, for $\Delta T \neq 0$, the curve crosses the horizontal axes at $\Delta V = V_0 = -S\Delta T$ (see Fig. 11 and eqn (4)). In practice, the voltage is ramped typically between $+10$ and -10 mV and the IV is recorded and processed to obtain the crossing point and the slope. Additionally, the conductance is also obtained from the current during the approach. Using this technique, further questions, like the effect of strain on the thermopower of the junction, can be explored. For more details, see below in Section 3.4.

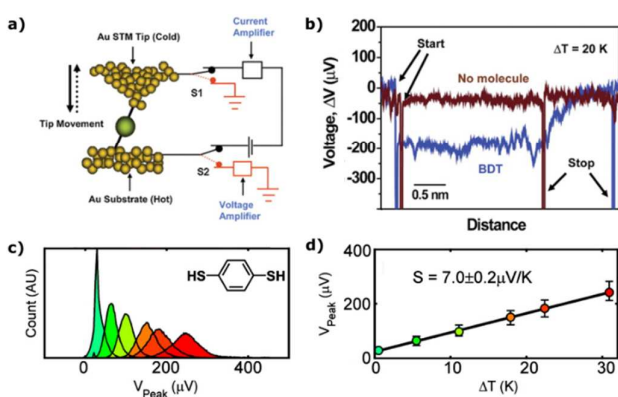**3.3 STM-BJ experimental results**

Fig. 9 First thermopower measurements in single-molecule junctions. (a) Schematic representation of the modified STM: a second mode is added to amplify the voltage between tip and substrate (red circuit) after the bias voltage and current amplifier are disconnected (black circuit). (b) Examples of individual traces obtained with the direct thermovoltage measurement technique of 1,4-benzenedithiol (BDT) molecular junctions. In this case, the thermovoltage is measured for a temperature gradient $\Delta T = 20$ K, while breaking the Au-BDT-Au junction (blue) and on clean Au substrate, without the molecule (red). (c,d) Linear dependence of the thermovoltage measurements on ΔT. The thermopower of the molecular junctions is found from the slope of V_{peak} vs. ΔT (d), where V_{peak} is the mean value of the thermovoltage histograms built with the individual traces (c). (a,b) From ref. 30. Adapted with permission from AAAS. (c,d) Adapted with permission from ref. 51. Copyright 2008 American Chemical Society.
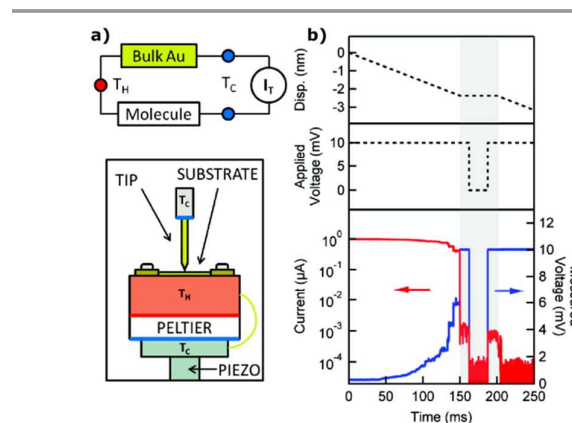

Fig. 10 STM-BJ-based technique for thermoelectric current measurements in molecular junctions. (a) Schematic representation of the experimental setup (bottom) and thermal circuit to be considered (top). (b) Measurement procedure: while the tip is withdrawn, its position is hold for 50 ms and the thermoelectric current is measured for 25 ms with no external voltage applied. The bias voltage is applied in series with a 10 KΩ resistor. In this case, the temperature gradient is established using a Peltier element instead of resistive heating. Curves with a similar conductance at the beginning and at the end of the hold period are considered to correspond to molecular junctions. Reprinted with permission from ref. 31. Copyright 2012 American Chemical Society.
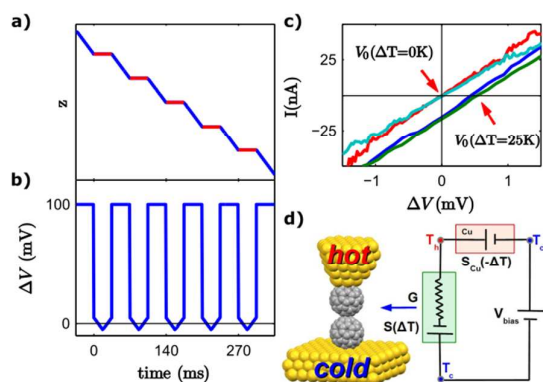
Fig. 11 Technique for the simultaneous measurement of thermopower and conductance. (a,b) Tip displacement z and bias voltage applied at the molecular junction, respectively, as a function of time. In each approaching–separating cycle, $50 - 100$ IV traces are acquired. (c) Experimental IV curves showing the voltage offset due to the temperature difference. (d) Schematic representation of the setup. The tip is heated to a temperature T_h above ambient temperature T_c while the substrate is maintained at room temperature T_c. Adapted with permission from ref. 32. Copyright 2013 American Chemical Society.

A number of interesting questions concerning the thermoelectric properties of molecular junctions have been addressed during the last years using the STM-BJ technique, such as the stability of the measurements, the molecular length dependence of thermopower, the effect of modifications in the structure of the backbone of the molecule or of the anchor groups, or the influence of electrode material.

The stability of the measurements is one of the earlier aspects discussed.[52-55] The thermopower of any given junction is remarkably stable, however, the thermopower values of different junctions are broadly distributed. Studying the thermopower experimentally and theoretically for different realizations of the same junction, it can be concluded that contact geometry, orbital hybridization, and intermolecular interactions result in variations in the alignment of the molecular level with the Fermi level of the electrodes and hence in variations of the thermopower (see Fig. 12). The observed increase in the width of the distribution with molecular length can be attributed to the larger number of available configurations.[52]

The thermopower dependence on the molecular length has been extensively studied and found to be linear in most of the cases. For example, in the case of oligophenyl molecules, the thermopower increases linearly with the number of oligomers for a given family of molecules with the same anchor group, while the conductance decreases exponentially. This is due to the fact that the frontier molecular orbitals shift closer to the Fermi level, but become more decoupled from the electrodes, as the molecular length increases (for further details, see Table 2). [30,56-58] Widawsky *et al.*,[59] on the other hand, observed an exponential increase due to the particular linking nature, as we will discuss later in this section (see Table 2). Recently, the role of the molecular backbone length has been analysed for an oxidized oligothiophene family, using the direct thermoelectric current measurement technique.[60] Interestingly, the results show that molecular transport is

greatly influenced by the molecular length to the point that a charge carrier change is observed for the longest molecule (see Table 2).

Understanding the role played by the chemical structure of the molecule on the thermopower can be used to tune and enhance the thermoelectric properties of molecular junctions. One strategy consists in the shifting of the frontier molecular orbitals with respect to the Fermi level by modifying the molecular backbone,[51,56,57] by changing the anchor groups,[31,51,56] or by atom encapsulation.[61,62]

With respect to the molecular backbone, the strategies explored involve the addition of electron-withdrawing or -donating side groups, or the modification of its conjugation. For example, it has been shown that the addition of electron-donating side groups in the backbone generally results in enhanced G and S properties when transport takes place though the HOMO, while electron-withdrawing units have the opposite effect. This is because electron-donating side groups increase the electron density of the system, thus the energy of the HOMO increases and shifts closer to the Fermi level (see Table 2).[51] Similarly, incorporating π-conjugated elements (with lower tunnelling barriers) in the backbone results in a linear increase of the thermopower, and the opposite by incorporating alkane units due to the localization of the molecular orbitals. In both cases, conductance decreases exponentially with the molecular length, as already discussed above.[56,57]

Usually, the tunability offered by backbone modification with side groups is limited compared with variations induced by different anchor groups. Anchor groups are known to play a key role in the realignment of the molecular orbitals during the junction formation, so their influence has been widely explored. Transport through the HOMO or the LUMO, that is, p- or n-type, and hence the sign of the thermopower, is mainly determined by the nature of the anchor groups chosen to connect with the molecule.[51,56] They can also facilitate the tunability of the thermoelectric characteristics without major variations in the conductance (see Fig. 13) (see Table 2).[31] A remarkable increase in conductance and thermopower has been observed for a special case of molecules binding through
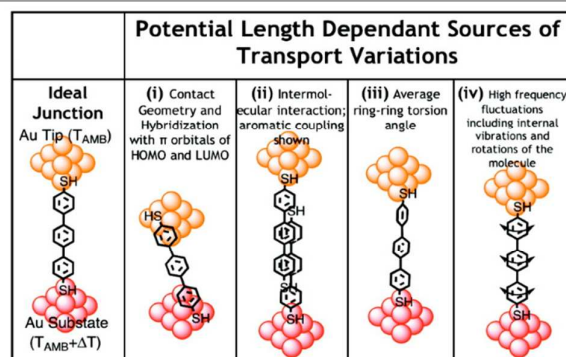

Fig. 12 Transport fluctuations. Possible origins of transport fluctuations from junction-to-junction. Contact geometry (i) and intermolecular interaction (ii) are the dominating sources of thermopower variations. These effects have higher variability for longer molecules. Reprinted with permission from ref. 52. Copyright 2009 American Chemical Society.
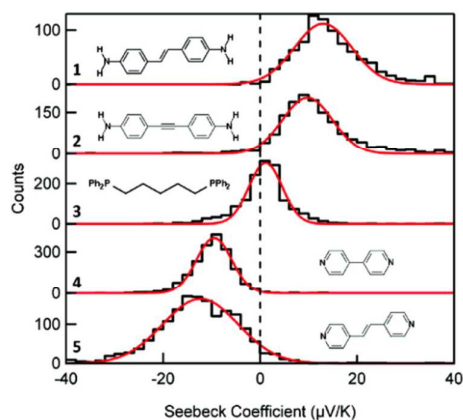
Fig. 13 Histograms of Seebeck coefficients for five different molecules. The effect of the anchor group on the transport properties of π-conjugated and non-conjugated molecular junctions have been studied. Reprinted with permission from ref. 31. Copyright 2012 American Chemical Society.

direct covalent Au-C sigma bonds.[59]

The results presented in ref. 56, in particular, reflect precisely the influence of these different variable characteristics of molecular design: thermopower varies linearly with the molecular length, increasing or decreasing depending on the nature of the molecular backbone, while the anchor group determines the so-called zero-length contact values (see Fig. 14). These different aspects of thermoelectricity in molecular junctions are summarized in the review by Malen *et al.*,[63] where a detailed theoretical background and an outlook on thermoelectric materials efficiency are also included.

Very recently, it has been shown that encapsulated atoms in fullerene cages can tune significantly their thermoelectric properties (see also section 3.4).[61,62]

Another factor that has been investigated, which affects transport properties in molecular junctions, is the material of the electrodes used to contact the molecules. Although gold electrodes are the most commonly used, platinum, silver, or
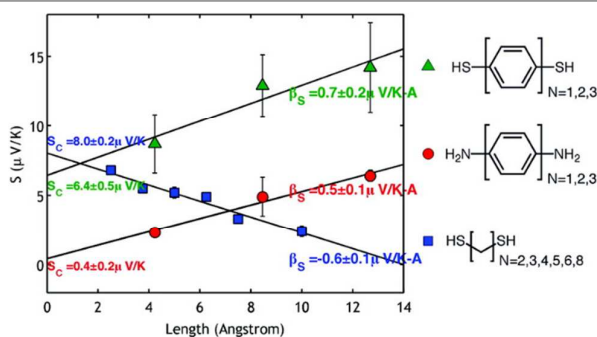

Fig. 14 Thermopower linear dependence on the molecular length and effect of the chemical nature of the backbone and the anchor groups. The molecular backbone determines the trend of S with length (increasing for phenyl rings and decreasing for alkane units), while the anchor groups fix the zero-length contact values (higher for thiol-anchored molecules compared with amine-anchored, due to the strong S-Au bond). Note that the term "zero-length" refers to the length of the molecule formed just by the anchor groups. Reprinted with permission from ref. 56. Copyright 2009 American Chemical Society.
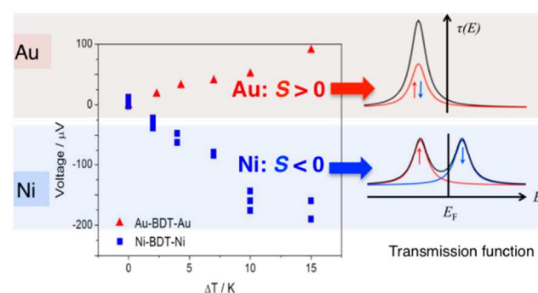

Fig. 15 Thermovoltage measurements in BDT junctions formed with Au (red triangles) and Ni (blue square) electrodes. The different sign of the thermovoltage is explained by the strong spin hybridization of the HOMO level of Ni-BDT-Ni junctions (right panel). Reprinted with permission from ref. 65. Copyright 2014 American Chemical Society.

nickel electrodes have been also used in a few cases (see Table 2).[58,64,65] Yee *et al.*[64] reported measurements of fullerene molecules (C_{60}, PCBM, and C_{70}) trapped between electrodes of different materials (Pt, Au, Ag). These molecules show larger (among the highest values measured up to date) thermoelectric coefficient than oligomers. Although the thermopower of these fullerenes is very robust and always negative, the electrode choice offers certain S tunability based on the different realignment of the molecular orbitals depending on the specific work function of the material. Lee *et al.*[65] have investigated the effect of ferromagnetic electrodes (*i.e.* Ni) and observed a strong spin hybridization of the HOMO level of BDT junctions which produces a change of the thermopower sign, compared with Au junctions, demonstrating new options for the tunability of the Seebeck coefficient (see Fig. 15).

Interestingly, the simple Lorentzian model introduced in Section 2 has been successfully used to elucidate molecular level alignment, yielding good agreement with the experiments.[51,52,54,56,58,64-66] Despite the suitability of this approach, modelling the thermoelectric properties of some molecules, like amine-terminated oligophenyls, can become very challenging because their transmission varies significantly from the Lorentzian form.[66]

3.4 STM imaging and simultaneous measurement of conductance and thermopower

The imaging capability of the STM has been also used to target single isolated molecules and to create well-defined single-molecule junctions. In 2013, Evangeli *et al.*[32] reported simultaneous conductance and thermopower measurements in single-molecule junctions formed after imaging individual molecules on an Au surface (see Fig. 16).

The simultaneous conductance and thermopower measurements were performed using the *IV* curves technique detailed in section 3.2.2. In Fig. 17, two examples of G and S measurements in C_{60} molecular junctions are shown. These results demonstrate that changes in the structure of the contact (atomic reorganizations in the electrodes) are reflected not only as jumps in the conductance but also, naturally, in the thermopower. It is also possible to locate isolated molecules and made a truly single-molecule contact.
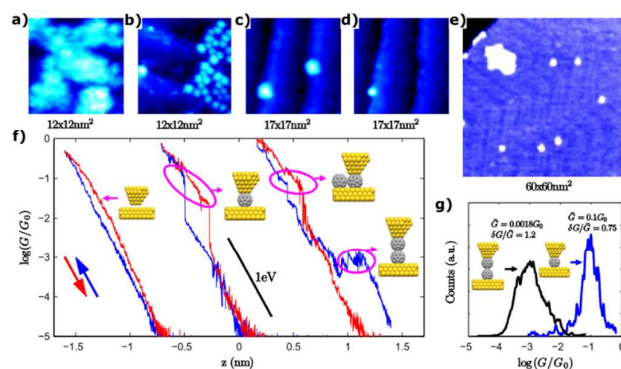
Fig. 16 Imaging technique. (a-e) STM topographic images of C_{60} molecules on Au (111). Small cluster imaged with a bare gold tip (a) and a C_{60}-tip (b), respectively. (c) Two C_{60} molecules imaged with a bare gold tip. (d) The same area shown in (c) after one of the molecules has been picked up by the tip. (e) Large area scan showing C_{60} molecules on a terrace and at step edges. (f) Approach (blue) and retraction (red) conductance curves for a bare gold tip on bare gold (leftmost traces); bare gold tip on an isolated C_{60} molecule (central traces); and C_{60} tip on an isolated C_{60} molecule (rightmost traces). The point of contact for a single C_{60} and for the C_{60} dimer are shown. (g) Histograms of the conductance of a bare gold tip on an isolated C_{60} molecule (blue curve) and of the conductance of a C_{60} tip on an isolated C_{60} molecule (black curve) at the points where contact is established. Adapted with permission from ref. 32. Copyright 2013 American Chemical Society.
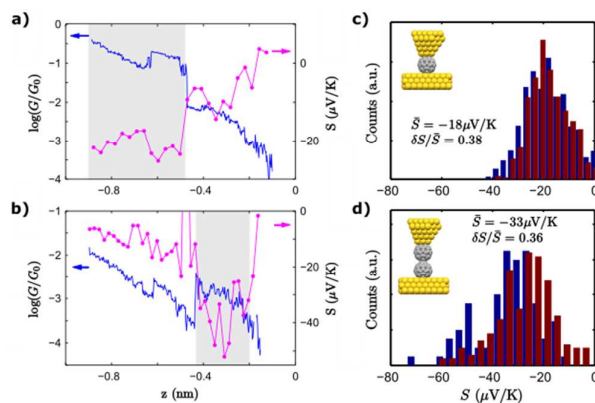

Fig. 17 Simultaneous conductance and thermopower measurements of individual junctions. (a,b) Conductance (blue) and thermopower (magenta) vs. tip displacement traces for single (a) and double (b) C_{60} fullerenes junctions. (c,d) Histogram of thermopower values for single (c) and double (d) C_{60} junctions, measured at $\Delta T = 12$ K (blue) and 25 K (red). Note that the thermopower of double C_{60} junctions is almost double than the single C_{60} junctions. Adapted with permission from ref. 32. Copyright 2013 American Chemical Society.

By picking up a molecule with the tip, 2-molecule junctions have been also formed, showing a thermopower that almost doubles that of a one-molecule junction, which is consistent with a two barriers in series model, for which the transmission is $\mathcal{T}(\varepsilon_F) \approx \mathcal{T}_1(\varepsilon_F)^2$ and, according to eqn (11), $S \propto \mathcal{T}'(\varepsilon_F)/\mathcal{T}(\varepsilon_F) = 2\mathcal{T}_1'(\varepsilon_F)/\mathcal{T}_1(\varepsilon_F)$ and hence $S \approx 2S_1$ (Fig. 17c,d).[1,10,32]

The power of the technique, in the case of fullerene molecules, became evident in the study of endohedral fullerenes (see Fig. 18).[62] It was observed that the sign of the thermopower depends specifically on the molecule that is probed, and interestingly could be correlated to the
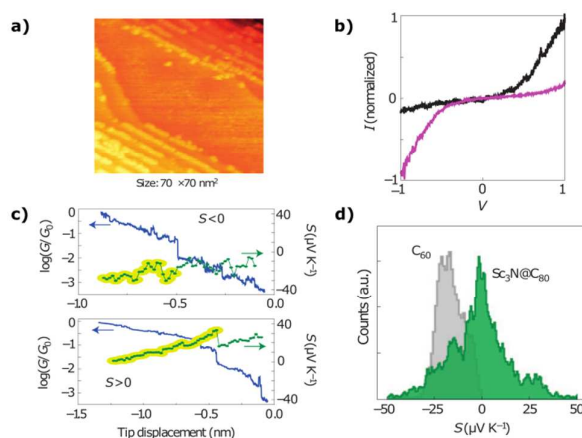

Fig. 18 Endohedral fullerenes. (a) STM images of the molecules on a flat Au (111) surface. (b) *IV* characteristics of two different molecules with different rectifying behaviour. (c) Examples of individual G (blue) and S (green) simultaneous measurements in two different molecules, showing distinct sign of the thermopower. The contact part is marked in yellow. (d) Histograms of the thermopower S at first contact for $Sc_3N@C_{80}$ (in green) compared to the values for C_{60} (in grey). Adapted by permission from Macmillan Publishers Ltd: Nature Materials (ref. 62), copyright 2015.

asymmetry of the *IV* curves in tunnelling (see Fig. 18b). Using DFT calculations, it was shown that the sign and magnitude of the thermopower depends on the orientation of the Sc_3N moiety inside the molecule with respect to the substrate. All this information is not obvious in the conventional histogram, which is centred on zero, but on the evolution of individual junctions (see Fig. 18c,d). Furthermore, the thermopower was found to be very sensitive to pressure, in particular, by performing small amplitude compression cycles on the molecule by the tip, it was observed that the conductance increases and thermopower decreases as the tip presses the molecule. The theoretical calculations showed that this sensitivity is due to the modification of coupling and the presence of a resonance very close to the Fermi level (see Fig. 19). Variations in the thermopower with strain in junctions of helicene molecules had been predicted theoretically,[67] although the mechanism involved is different.

3.5 Thermopower measurements using MCBJ

The MCBJ technique, widely used for conductance characterization of molecular junctions, has been also adapted for thermoelectric measurements. Compared to STM-BJ, this technique has the advantage of a larger mechanical stability. Its more important drawback is the slowness of junction formation, which hampers the gathering of large statistics.

The group of M. Taniguchi modified a lithographic MCBJ setup by placing a nanofabricated microheater made of a Pt coil adjacent to one side of the Au junction to create a thermal gradient.[33,68] They measured the thermopower and conductance of the junctions simultaneously by measuring the current and voltage drop in an external resistance connected in series to the junction (see Fig. 20). Using this technique, they characterized the thermoelectric properties of Au-1,4-
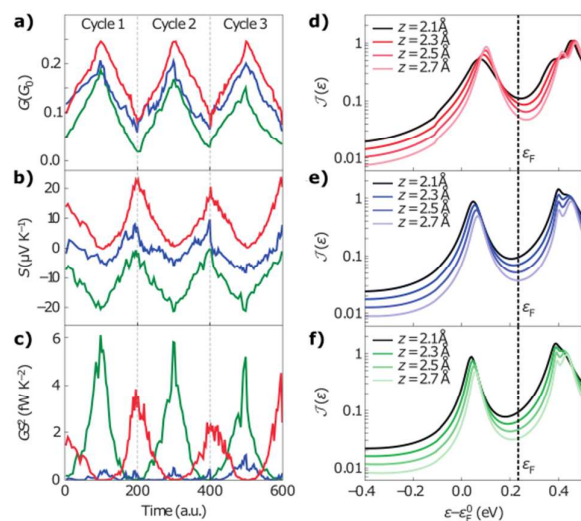
Fig. 19 Effect of pressure on $Sc_3N@C_{80}$ molecular junctions. (a–c) Periodical variations of the conductance G, thermopower S, and power factor GS^2, as the STM tip advances and retracts during three cycles. Each half cycle corresponds to less than 0.5 nm. Each colour corresponds to a different molecule. (d-f) Calculated transmission curves, $\mathcal{T}(\varepsilon)$, for three different orientations of $Sc_3N@C_{80}$. The Fermi level is shifted from the position given by DFT calculations and the black dotted line indicates the true Fermi level which reproduces the experimental behaviour of thermopower as the molecule is pressed. Adapted by permission from Macmillan Publishers Ltd: Nature Materials (ref. 62), copyright 2015.

benzenedithiol(BDT)-Au junctions and of Au atomic contacts (see section 4 for further details about metallic contacts).[33,69]

Notched-wire MCBJ have been also adapted to measure thermopower. Apart from the pioneering experiment on the thermopower of metallic contacts,[70] which we will describe in detail in Section 4, BDT molecular junctions have been investigated.[34]

3.6 Conducting ThAFM

An AFM technique for thermoelectric characterization of molecular junctions, thermoelectric AFM (ThAFM), was introduced by the group of P. Reddy in 2010.[36] It is based in the conducting probe AFM (CP-AFM) technique, pioneered by Frisbie *et al.*,[71] which has been used to characterize the conductance of molecular junctions formed on a SAM. In the ThAFM, an electrical heater is attached to the gold substrate to establish the temperature gradient. The silicon cantilever is gold coated and is anchored to a thermal reservoir at constant temperature. The large thermal conductivity of silicon ensures that at least 95% of the temperature drop is at the junction. As in the STM technique presented by the same group,[30] either current or voltage can be measured by switching circuits (see Fig. 21).

The ThAFM has been used to probe the dependence of junction thermoelectric properties on molecular length and contact coupling chemistry using a combined experimental and computational approach.[36,72-75] The molecular junction was formed by placing the AFM tip in soft mechanical contact with the SAM. The force exerted by the tip was set to ~1 nN and approximately100 molecules were probed simultaneously
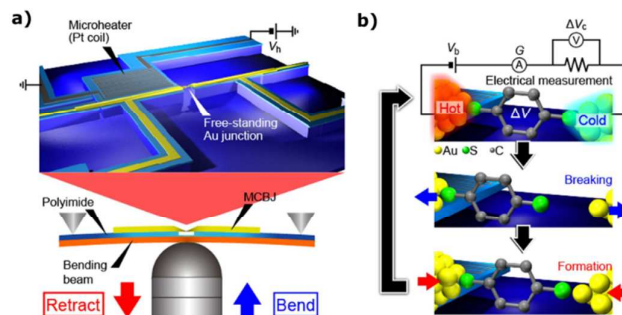

Fig. 20 Microheater-embedded lithographic MCBJ technique for measuring thermopower and conductance in molecular junctions.[33,68] (a,b) Schematic illustration of the technique (a) and of the measurement procedure (b). The thermopower and conductance are measured simultaneously by measuring the current and the voltage drop on an external resistor. Reprinted with permission from ref. 68.
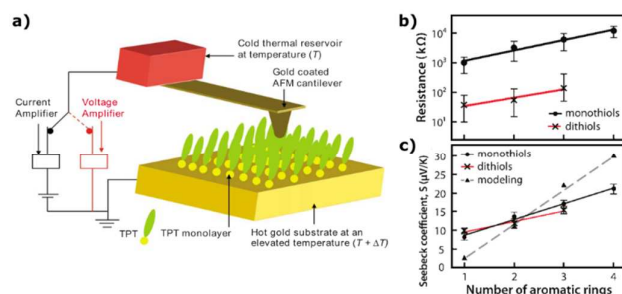

Fig. 21 ThAFM technique for measuring thermopower of SAMs. (a) Schematic of the technique. Molecules form a SAM on an Au substrate and the Au coated cantilever tip is placed in contact with them. The tip is in contact with a thermal reservoir at temperature T, while the substrate to a temperature $T + \Delta T$. Current or voltage of the junction can be measured by switching to the adequate amplifier. (b,c) Electrical resistance (b) and Seebeck coefficient (c) of monothiols and dithiols junctions of ~100 molecules obtained with ThAFM technique. The calculated Seebeck coefficient for the dithiol junctions is also plotted. (a) Adapted with permission from ref. 36. Copyright 2010, AIP Publishing LLC. (b,c) Adapted with permission from ref. 72. Copyright 2011 American Chemical Society.

as estimated from the characterization of the tip shape. The larger contact areas provide higher stability and larger currents, facilitating voltage dependence studies and the possibility of measuring longer molecules. The values obtained for the thermopower in dithiol terminated oligophenyl molecular junctions were in very good agreement with those reported in single-molecule junctions, indicating that, in this case, the lateral interactions were negligible (see Section 2). It was also found that, in the case of monothiol junctions, the electrical conductance decreases more than an order of magnitude, while the thermopower values remain similar, compared with the dithiol junctions (see Table 2). This behaviour can be understood considering that monothiol- and dithiol-terminated molecules are essentially weakly and strongly coupled, respectively.

3.7 Electromigrated break junctions

In contrast to all previously presented techniques which are two-terminal techniques, electromigrated break junctions can be provided with a third electrode acting as an electrostatic

gate, which makes possible to modify the alignment of the molecular levels. In this technique, a nanogap is created by passing a high current through an e-beam lithographically defined gold wire sitting on top of a gate electrode. The nanogap must be of molecular dimensions, which requires a careful control of the current during the process.[76,77] In general, the molecules are deposited on the wire prior to breaking. The main drawback of this technique is that the separation of the electrodes, once the gap has been created, cannot be altered. In addition, the yield of successful molecular junctions is reduced.

A modified electromigrated break junction provided with an integrated heater has been demonstrated by the group of
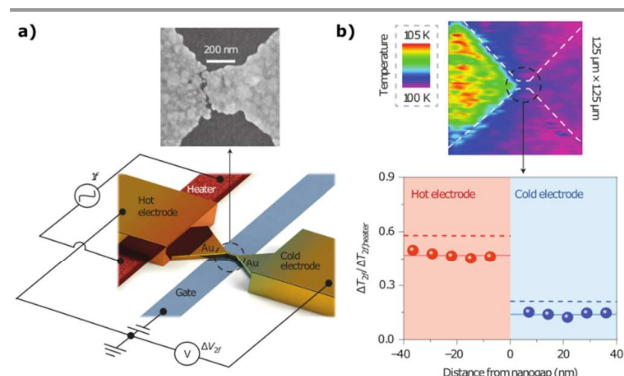

Fig. 22 Experimental setup for tuning the thermoelectric properties of molecular junctions. (a) Schematic of the electromigrated break junctions with integrated heater. (b) Thermal characterization of the device: SThM thermal image of the nanogap at 100K (top) and normalized temperature profile in the vicinity of the nanogap junction (down) measured by SThM (circles) and by theoretical modelling (dotted). Adapted by permission from Macmillan Publishers Ltd: Nature Nanotechnology (ref. 35), copyright 2014.
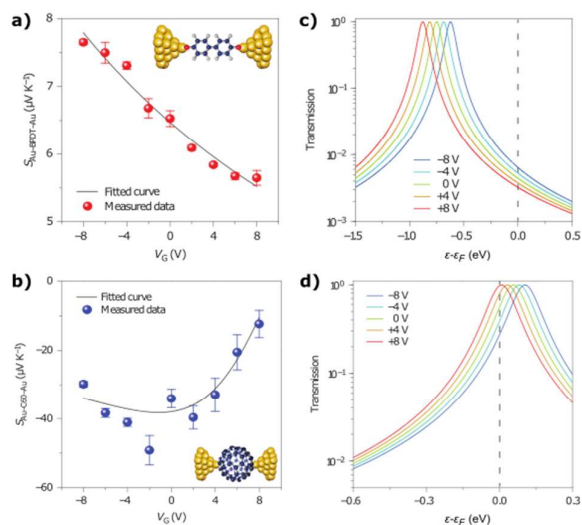

Fig. 23 Effect of tuning the electronic structure on the thermoelectric properties of Au-BPDT-Au and Au-C_{60}-Au junctions. (a,b) Measured Seebeck coefficient *versus* V_G for BPDT (a) and C_{60} (b) junctions. Solid line is the least-squares fit of eqn (19). (c,d) Transmission functions for different V_G values calculated from eqn (18) for BPDT (c) and C_{60} (d) junctions. The Fermi level is indicated with a dotted line. Adapted by permission from Macmillan Publishers Ltd: Nature Nanotechnology (ref. 35), copyright 2014.

P. Reddy.[35] After careful testing to ensure the existence of an abrupt temperature gradient at the junction (see Fig. 22), molecular junctions of BPDT and C_{60} were studied using this setup at 100 K in vacuum. Their behaviour with gate voltage was quite distinct: for increasing gate voltage, the conductance and thermopower of BPDT decreased, while for C_{60} they show a non-monotonic behaviour (see Fig. 23). This behaviour can be understood taking into account that the molecular levels shift with respect to the Fermi level as the gate voltage is applied. In a one level model (that takes into account only transport through the dominant molecular level, *cf.* eqn (12)), we can introduce the effect of the gate voltage on the molecular junction. If V_G is the gate voltage and α is the effectiveness of the gate coupling, we may write the transmission of the junction as

$$\mathcal{T}(\varepsilon, V_G) = \frac{4\Gamma_L\Gamma_R}{[\varepsilon-(\varepsilon_0-\alpha V_G)]^2+(\Gamma_L+\Gamma_R)^2} \qquad (18)$$

and the gate dependent Seebeck coefficient as

$$S(T) = -\frac{\pi^2}{3}\frac{k_B^2 T}{e}\frac{\mathcal{T}'(\varepsilon_F)}{\mathcal{T}(\varepsilon_F)} = -\frac{\pi^2}{3}\frac{k_B^2 T}{e}\frac{2[\varepsilon_F-(\varepsilon_0-\alpha V_G)]}{[\varepsilon_F-(\varepsilon_0-\alpha V_G)]^2+(\Gamma_L+\Gamma_R)^2}. \qquad (19)$$

By fitting the experimental data with eqn (19), they obtained values for Γ, ε, and α and then the transmission function was calculated. For BPDT (HOMO dominated transport), swiping the voltage from positive to negative results in a shift of the resonance peak further away from ε_F, while for C_{60} (LUMO dominated transport) closer to ε_F (see Fig. 23c,d). In the case of C_{60}, since transport is very close to the resonance, these small shifts produce a different dependence of S with V_G than for BPDT (see Fig. 23d).

These results are a demonstration of the direct relation between charge transmission and thermoelectricity in molecular junctions.

3.8 Nanoparticle arrays

Arrays of nanoparticles or nanocrystals stabilized with organic surface ligands constitute a multidimensional network of molecular junctions. These 3D or 2D arrays of semiconducting and metallic subnanometric particles present diverse electronic and optoelectronic properties,[78,79] which can be tuned by varying the nanoparticle material, the interparticle distance, and the organic ligands, making them very attractive for their potential to implement molecular junctions in devices for practical applications.

Müller considered theoretically a 3D array consisting in silicon nanoparticles connected by molecular junctions.[80] He showed that in the ideal case, in which all junctions are identical, the conductance and thermopower of the array could be written as

$$G = \frac{M\,G_J N_{CS}}{N_T}, \qquad (20)$$

$$S = S_J, \qquad (21)$$

where N_{CS} and N_T are the number of junctions in the cross section of the film and in the direction of transport, respectively; M is the number of molecules in a junction, and

G_J and S_J are the conductance and thermopower of a single-molecule junction, respectively.

Chang et al.[37] used nanocrystal arrays of gold particles to test the thermoelectric properties of molecular junctions (see Fig. 24). The arrays were synthesized in oleylamine ligands and deposited as films of $1\,\mu m$ thickness and millimetric lateral dimensions. The Au nanocrystals were 7 nm in diameter and the ligand molecules were exchanged by various monothiol and dithiol molecules of different lengths. The ligand length dependence of the conductance and thermopower measured in these films was in partial agreement with the values obtained in single-molecule junctions; however, some of the observations, like the opposite sign of the thermopower for alkanedithiols and the enhanced thermopower showed by oligophenyldithiol ligands, require further investigation.

Experimental results for 2D arrays have not yet been reported, but the possibility of gating the array electrostatically is very attractive.
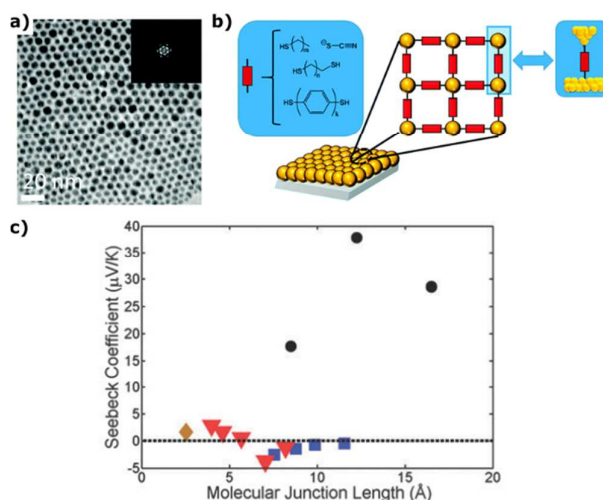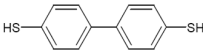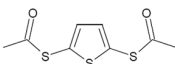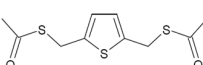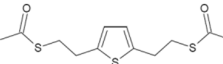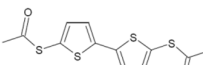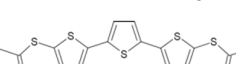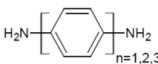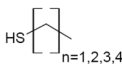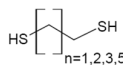

Fig. 24 Nanoparticle arrays technique for thermoelectric measurements. (a) Transmission electron microscopy image of gold nanocrystal arrays with oleylamine ligands and Fourier transform of the image as an inset. (b) Schematic representation of gold nanocrystal arrays with organic surface ligands. Chemical structures of the ligands used: monothiol terminated (thiocyanate and alkanethiols) and two types of dithiol terminated (alkanedithiols and oligophenyldithiols). (c) Seebeck coefficient of the gold nanocrystal arrays *versus* ligand length for thiocyanate and alkanethiols (red triangles), alkanedithiols (blue squares), and oligophenyldithiols (black circles). Adapted from ref. 37 with permission from the PCCP Owner Societies.
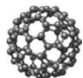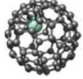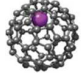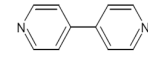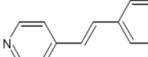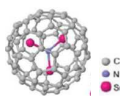
Table 2 Conductance G and thermopower S values measured up to date in molecular junctions. The error in the thermopower measurement ΔS is also included in some cases. The metallic electrodes are gold (Au) except when explicitly indicated.
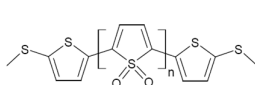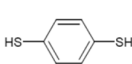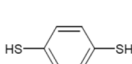
Molecule	Schematic of the molecule	G (G_0)	S, ΔS ($\mu V\,K^{-1}$)	Purpose of the experiment and reference
1,4-benzenedithiol (BDT)			8.7 ± 2.1	
4,4'-dibenzenedithiol (DBDT)			12.9 ± 2.2	First measurement of the Seebeck coefficient of molecular junctions; length dependence of S.
4,4''-tribenzenedithiol (TBDT)			14.2 ± 3.2	Ref. 30
1,4-benzenedithiol (BDT)		$1.05 \cdot 10^{-2\ a}$	7.2 ± 0.2	
2,5-dimethyl-1,4-benzenedithiol (BDT2Me)		$1.19 \cdot 10^{-2\ a}$	8.3 ± 0.3	
2,3,5,6-tetrachloro-1,4-benzenedithiol (BDT4Cl)		$7.6 \cdot 10^{-3\ a}$	4.0 ± 0.6	Effect of the chemical structure on the molecular junction transport properties: addition of substituents to BDT and variation of the anchor group.
2,3,5,6-tetrafluoro-1,4-benzenedithiol (BDT4F)		$8.7 \cdot 10^{-3\ a}$	5.4 ± 0.4	Ref. 51
1,4-benzenedicyanide (BDCN)			-1.3 ± 0.5	

Molecule	Structure		Description
1,4-n-phenylenedithiol (PDT) (n = 1,2,3)		8.7 ± 2.1 $\quad$ 12.9 ± 2.2 $\quad$ 14.2 ± 3.2	Molecular length influence in the orbital alignment and the contact coupling of the junctions. Ref. 56
1,4-n-phenylenediamine (PDA) (n = 1,2,3)		2.3 ± 0.3 $\quad$ 4.9 ± 1.9 $\quad$ 6.4 ± 0.4	
n-alkanedithiol (ADT) (n = 2,3,4,5,6,8)		6.8 ± 0.2 $\quad$ 5.5 ± 0.1 $\quad$ 5.2 ± 0.4 $\quad$ 4.9 ± 0.2 $\quad$ 3.3 ± 0.1 $\quad$ 2.4 ± 0.4	
1,4-benzenedithiol (BDT)		7.7 ± 0.5	Study of thermopower variations; length dependence of these fluctuations. Ref. 52
4,4'-dibenzenedithiol (DBDT)		10.8 ± 0.6	
4,4''-tribenzenedithiol (TBDT)		15.1 ± 0.9	
2',5'-dimethyl-4,4''-tribenzenedithiol (DMTBDT)		15.9 ± 2.5	
1,1',4',1''-terphenyl-4-thiol (TPT) (SAM)		16.9 ± 1.4	AFM-based technique to identify orbital alignment in a self-assembled monolayer (SAM). Ref. 36
1,4-n-benzenedithiol (n-BDT) [Dithiol terminated aromatic molecules (n = 1,2,3)] (SAM)		9.8 ± 0.6 $\quad$ 11.7 ± 1.3 $\quad$ 15.4 ± 1.0	Length and contact coupling-strength dependence of SAMs' thermoelectric properties. Ref. 72
1-n-benzenethiol (n-BT) [Single thiol terminated aromatic molecules (n = 1,2,3,4)] (SAM)		8.1 ± 0.8 $\quad$ 13.6 ± 1.2 $\quad$ 17.0 ± 1.0 $\quad$ 21.0 ± 1.3	
1-tribenzenecyanide (TBCN) [Isocyanide (-NC)-terminated aromatic molecules] (SAM)		−1.0 ± 0.4 $\quad$ −1.6 [b]	

Molecule	Structure	Value 1	Value 2	Description
Au substrate - C_{60} - Pt tip		~7.1 · 10^{-4}	−8.9 ± 2.2	
Au substrate - C_{60} - Au tip		~2.5 · 10^{-4}	−14.5 ± 1.2	
Au substrate - C_{60} - Ag tip		~2.0 · 10^{-3}	−29.6 ± 3.4	
Au substrate -PCBM- Pt tip (PCBM ≡ [6,6]-phenyl-C_{61}-butyric acid methyl ester)		~1.3 · 10^{-3}	−7.6 ± 3.2	Fullerene heterojunctions; effect of the electrodes material on the orbital alignment and coupling. Ref. 64
Au substrate -PCBM- Au tip		~2.5 · 10^{-3}	−16.4 ± 1.6	
Au substrate -PCBM- Ag tip			−30.0 ± 2.6	
Au substrate - C_{70} - Pt tip		~6.3 · 10^{-4}	−8.4 ± 1.9	
Au substrate - C_{70} - Au tip		~6.3 · 10^{-4}	−20.1 ± 1.4	
Au substrate - C_{70} - Ag tip		~1.6 · 10^{-3}	−33.1 ± 8.8	

Molecule	Structure	G	S	Notes
4,4'-diaminostilbene		$6.3 \cdot 10^{-4}$	13.0 ± 7.0	Amine-Au and pyridine-Au linked π-conjugated molecular junctions: effect of the anchor group on the transport properties; alkane molecules. Ref. 31
Bis-(4-aminophenyl)acetylene		$5.7 \cdot 10^{-4}$	9.7 ± 6.1	
1,5-bis-(diphenylphosphino)pentane		$3.9 \cdot 10^{-4}$	1.1 ± 4.1	
4,4'-bipyridine		$6.8 \cdot 10^{-4}$	9.5 ± 4.3	
1,2-di(4-pyridyl)ethylene		$2.4 \cdot 10^{-4}$	12.3 ± 9.1	
Fullerene C_{60}		$1 \cdot 10^{-1}$	-18 ± 6.84	Simultaneous measurement of G and S in fullerene junctions; thermopower enhancement by tuning the interaction between molecules. Ref. 32
Dimer C_{60}		$1.8 \cdot 10^{-3}$	-33 ± 11.88	
1,4-bis((trimethylstannyl)methyl)-n-phenyl (n = 1,2,3,4)		$9 \cdot 10^{-1}$ $1 \cdot 10^{-1}$ $1.4 \cdot 10^{-2}$ $2 \cdot 10^{-3}$	2.4 14.3 20.9 23.9	Length dependence thermopower of molecules binding to the electrodes through a covalent Au-C bond. Ref. 59
1,6-bis(trimethylstannyl)-n-alkanes (n = 6,8,10)		$1.4 \cdot 10^{-2}$ $2 \cdot 10^{-3}$ $3 \cdot 10^{-4}$	5.0 5.6 5.6	
4,7-dithiophenyl-2,1,3-benzothiadiazole-3',3''-dithiol (DTBTDT)		$9.2 \cdot 10^{-3}$	15.46 ± 0.15	STM-BJ technique; G and S measurements and transition voltage spectroscopy (TVS); thermopower dependence on energy level alignment. Ref. 54
1,4-butanedithiol (C4)		$4.5 \cdot 10^{-3}$	2.1 ± 0.11	
1,6-hexanedithiol (C6)		$6.2 \cdot 10^{-4}$	5.55 ± 0.13	
1,4'-biphenyldithiol (BPDT)		$7.5 \cdot 10^{-3}$	7.92 ± 0.14	
4,4'-dimercaptostilbene (DMS)		$5.2 \cdot 10^{-3}$	8.35 ± 0.23	
4,4'-bipyridine		$4 \cdot 10^{-4}$ (high G) $1 \cdot 10^{-4}$ (low G)	-8.4 -7.5	Orbital alignment and coupling of Au-bipyridine-Au junctions; two G states with different coupling strength; comparison with other pyridine-linked and amine-terminated molecules. Ref. 66
1,2-di(4-pyridyl)ethylene (BPE)		$2.8 \cdot 10^{-4}$ (high G) $7.5 \cdot 10^{-5}$ (low G)	-10.1 -9.3	
1,4-n-phenylenediamine (n = 1,2,3)		$6.25 \cdot 10^{-3}$ $1.10 \cdot 10^{-3}$ $1.6 \cdot 10^{-4}$	3.1 7.9 10.4	
1,4-benzenedithiol (BDT)		10^{-2}	1.4	G and S measurements of metallic and molecular junctions using a microheater-embedded MCBJ technique. Ref. 33
Au substrate - BDT - Au tip		$\sim 1 \cdot 10^{-2}$	7.44 ± 0.5	Influence of ferromagnetic electrodes on the thermoelectric properties of molecular junctions. Ref. 65
Ni substrate - BDT - Ni tip			-12.1 ± 1.3	
Au substrate - C_{60} - Au tip		$\sim 2 \cdot 10^{-1}$	-16.1 ± 0.5	
Ni substrate - C_{60} - Ni tip			-12.5 ± 1.2	

Molecule		Value 1	Value 2	Description
Biphenyl-4,4'-dithiol (BPDT)		[0.006, 0.003]	~[7.7, 6.7, 5.6]	Electrostatic gate control of transport properties on molecular junctions with three-terminal devices [$V_G = (-8, 2, 8)$ V]. Ref. 35
Fullerene C_{60}		[0.43, 0.65]	~[−30, −50, −12]	
S,S'-thiophene-2,5-diyl diethanethioate (T1)		0.0075	6.83	Thiophene-based heterojunctions; effect on transport properties of nonconjugated and π-conjugated molecular elements. Ref. 57
S,S'-thiophene-2,5-diylbis(methylene) diethanethioate (TA2)		0.0035	3.01	
S,S'-2,2'-(thiophene-2,5-diyl)bis(ethane-2,1-dyil) diethanethioate (TA3)		0.002	2.2	
S,S'-([2,2'-bithiophene]-5,5'-diyl) diethanethioate (OT2)		0.0031	7.49	
S,S'-([2,2:5',2''-terthiophene]-5,5''-diyl) diethanethioate (OT3)		0.0007	14.84	
Ag - n-oligophenyldiamine - Ag (n = 1,2,3)		− − $1.7 \cdot 10^{-4}$	2.1 6.3 8.7	Lower S for Ag than for Au in HOMO dominated transport due to the lower work function of silver. Ref. 58
Au - n-oligophenyldiamine - Au (n = 1,2,3)			~3.5 ~8.0 ~10.5	
Au NCA- n-alkanethiol -Au NCA (n = 1-4)		~0.05 Ωm ~0.07 Ωm ~0.9 Ωm ~11 Ωm ~100 Ωm	~2.7 ~1.5 ~0.3 ~ − 3.8 ~ − 1.4	Scalability of molecular junctions to the macroscale through nanocrystal arrays (NCA). Ref. 37
Au NCA- n-alkanedithiol -Au NCA (n = 1, 2, 3, 5, 7)		~11 Ωm ~9 Ωm ~12 Ωm ~115 Ωm ~1300 Ωm	~ − 2.4 ~ − 1.5 ~ − 0.8 ~ − 0.5	
Au NCA- n-oligophenyldithiol -Au NCA (n = 1-3)		~0.2 Ωm ~0.4 Ωm ~0.3 Ωm	~17 ~38 ~26	
Oligomers of thiophene-1,1-dioxide (TDOn, n = 1,2,3,4)		$\sim 9 \cdot 10^{-4}$ $\sim 5 \cdot 10^{-4}$ $\sim 2 \cdot 10^{-4}$ $\sim 6 \cdot 10^{-5}$	7.3 6.4 2.4 −22.1	Length influence on thermoelectric properties of molecular junctions; the charge carriers depend on the backbone length. Ref. 60
1,4-benzenedithiol (BDT)		$1 \cdot 10^{-2}$	~11	MCBJ technique and IETS (inelastic electron tunnelling spectroscopy) characterization for G and S measurements; negative correlation between G and S. Ref. 34
1,4-benzenedithiol (BDT)		$1.1 \cdot 10^{-2}$	15 ± 4	Thermopower sensitivity on molecular bridge geometrical configurations. Ref. 68

Fullerene C_{82}		$\sim 2 \cdot 10^{-1}$	-22.7 ± 0.9	
Endohedral fullerene Gd@C_{82}		$\sim 2 \cdot 10^{-1}$	-31.6 ± 1.2	STM-BJ measurements of G and S in endohedral metallofullerenes junctions; modified thermopower compared to the pristine C_{82}. Ref. 61
Endohedral fullerene Ce@C_{82}		$\sim 2 \cdot 10^{-1}$	-30.0 ± 1.0	
4,4'-bipyridine (BPy)		$\sim 5 \cdot 10^{-4}$ (high G) $\sim 1.5 \cdot 10^{-4}$ (low G)	-8.2 -8.4	Effect of different interactions (van der Waals and donor-acceptor) in the S distribution of single-molecule junctions. Ref. 55
1,2-bis(4-pyridyl)ethylene (BPyE)			-9.0 -9.3	
Endohedral fullerene $Sc_3N@C_{80}$		$5 \cdot 10^{-2}$	From -25 to $+25$ (orientation dependent, see Fig. 18d)	G and S simultaneous characterization of individual endohedral fullerenes: bi-thermoelectricity depending on the orientation of the molecule and pressure. Ref. 62

^{a} G calculated from S using theoretical models. ^{b} Theoretically calculated value.

4. Metallic contacts

Atomic contacts are a paradigm in quantum transport and have played an important role in the understanding of physics at the nanoscale. The first measurement of thermopower in metallic contacts was reported in 1999 by the group of J. M. van Ruitenbeek, almost a decade earlier than the first thermopower measurements in molecular junctions.[70] They used a notched-wire MCBJ setup to form atomic-size contacts in a thin gold wire provided with thermometers and heaters at both ends. The experiments were performed at liquid helium temperatures (see Fig. 25a).

The conductance traces (see Fig. 25b) show characteristic plateaus, corresponding to stable atomic configurations, separated by abrupt jumps caused by sudden atomic
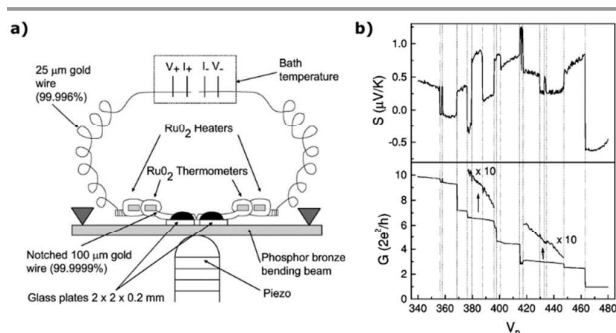

Fig. 25 Thermopower of atomic-size Au contacts using a MCBJ setup at helium temperature. (a) Schematic of the modified MCBJ setup used for conductance and thermopower simultaneous measurements of atomic contacts. (b) Examples of thermopower S (top panel) and conductance G (bottom panel) traces during the last stages of breaking the Au metallic contact *versus* the piezovoltage V_p. Both positive and negative thermopower values were observed. Thermopower presents abrupt jumps coinciding with the ones of conductance. Reprinted figures with permission from ref. 70. Copyright 1999 by the American Physical Society.

rearrangements. The conductance of the last plateau before total rupture equals $1\, G_0$. The thermopower trace acquired simultaneously also present abrupt jumps indicating the sensitivity of thermopower to detailed atomic configurations. Quantum oscillations in the thermopower, predicted by the theory, were not observed, but the standard deviation of the thermopower presented a deep minimum at $G = G_0$.

In recent experiments in ambient conditions, Evangeli *et al.*[12] studied Au and Pt contacts starting with very large contacts $(G > 10^4 G_0)$, observing a crossover from bulk thermopower values (1 µV K^{-1} for Au and -4 µV K^{-1} for Pt) to values around -0.75 µV K^{-1} for Au and 1.1 µV K^{-1} for Pt as the contact size diminish to atomic dimensions (see Fig. 26). This observation clearly shows the different nature of bulk and nanoscale thermopower (as commented above, in Section 2). A phenomenological explanation can be given in terms of the electronic mean free path l and contact radius a. The conductance and thermopower are written as

$$G = xG_S + (1-x)G_M \qquad (22)$$

and

$$S = xS_S + (1-x)S_M, \qquad (23)$$

where $x = e^{-a/l}$; $G_M = 2a/\rho$ is Maxwell's spread conductance for large contacts, ρ being the resistivity of the metal; $G_S = G_0(k_F a/2)^2$ is Sharvin's conductance for contacts smaller than the mean free path, k_F being the Fermi wavenumber; and S_M and S_S are the bulk and nanoscale thermopowers, respectively. This expression indicates that the dominant transport mechanism change is determined by the ratio of the contact radius a to the mean free path l.

For contacts of atomic size, in the case of Au, quantum oscillations are observed with suppression of the
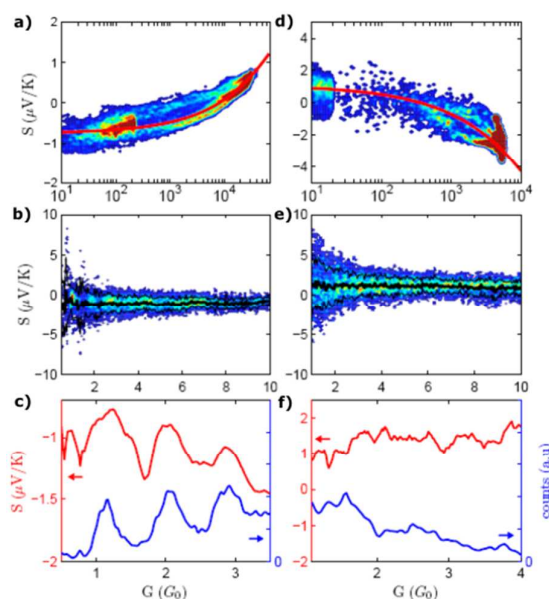
Fig 26 Thermopower of Au and Pt atomic-size contacts using STM at room temperature. (a,d) Density plots of the thermopower *versus* conductance for very large contacts of Au (a) and Pt contacts (d). Red thick lines show the fit that describes the transition between atomic contacts and bulk-like wires. The values used in the fit are the following: for Au, $S_S = -0.75\ \mu V\ K^{-1}$ and $S_M = 1.94\ \mu V\ K^{-1}$; for Pt, $S_S = +1.1\ \mu V\ K^{-1}$ and $S_M = -5.3\ \mu V\ K^{-1}$. The best fit was obtained for values of l of 37 and 14 nm for Au and Pt, respectively. (b,e) Thermopower density plots as a function of the conductance for small contacts up to $10G_0$ of Au (b) and Pt (e) contacts, respectively. The mean value of thermopower is negative for Au and positive for Pt. (c,f) Conductance histogram (blue) and average thermopower (red) for few atom contacts of breaking curves on Au (c) and on Pt (f). Reprinted with permission from ref. 12. Copyright 2015 American Chemical Society.

thermopower close to integer values of the quantum conductance (see Fig. 26c and also ref. 33 and 69). In contrast, these oscillations are not observed in the case of Pt contacts (see Fig. 26f). Molecular dynamics simulations[81] combined with DFT calculations[12] show that these differences have their origin in the different electronic structure of Au and Pt atomic contacts.

5. Conclusions and outlook

The measurement of thermopower in molecular junctions, first realised in 2007, has become an essential characterization tool for these systems. The techniques employed consist in adaptations of those used for investigating the electrical conductance. The main issues for this adaptation are the establishment of a well-defined temperature gradient, which is generally straightforward in the case of STM or AFM but quite challenging in others, such as lithographically fabricated systems, and the modifications in the electronics and data acquisition necessary to measure both conductance and thermopower.

From a fundamental point of view, the measurement of the thermopower of a molecular junction in addition to its conductance allows the comparison of state-of-the-art quantum transport theoretical calculations to experimental

results, providing deep insight into the electronic structure and transport properties of the junction. Basic questions such as the dependence of thermopower on the length of the molecule, the effect of the chemistry of the anchor groups and of the electrodes on the level alignment, and the modification of transport properties by the changes introduced in the backbone of the molecule have been addressed and are well understood.

From the point of view of applications, the utilization of molecular junctions in thermoelectric devices requires high thermoelectric efficiencies (characterised by a dimensionless figure of merit *ZT* larger than 1). Although *ZT* has not been directly determined in molecular junctions, the values of the thermopower and of theoretical estimates indicate that higher efficiencies are necessary. The enhancement of the thermoelectric efficiency presents three important challenges.

The first challenge is the exploration of heat transport at the nanoscale. Indeed, this topic has remained largely unexplored due to the experimental difficulties and the requirement of new exquisitely sensitive instrumentation. Although currently efforts are being made by several groups to measure heat conductance in molecular junctions, only measurements in SAMs have been reported so far.[82-84] A complete understanding of the interplay between electrical and thermal conductance is essential not only to develop efficient thermoelectric applications, but also for nanoscale electronics applications.

The second challenge is the enhancement of the thermoelectric efficiency. The most promising route, according to theoretical predictions,[10] which indicate that high efficiencies could be achieved, is the use of quantum interference introduced by chemical synthesis in the form of resonances. The effect of quantum interference on conductance has been reported[85] and recently the importance of resonances in determining the thermopower has been demonstrated.[62] Enhanced efficiencies could also result from the use of semiconducting electrodes, according to other theoretical predictions.[86,87]

The third challenge is the integration of molecular junctions in thermoelectric devices. A promising option is adopting a planar configuration in the form of a SAM sandwiched in between two electrodes. Advances in this direction have been made using graphene to protect the SAM.[88] Nanoparticle arrays are also an attractive geometry for device integration.

Our ability to address these challenges might lead to the creation of a viable technology platform for harvesting waste heat with an important economic impact.

Acknowledgements

Notes and references

1 J. C. Cuevas and E. Scheer, *Molecular Electronics: An Introduction to Theory and Experiment*, World Scientific, Singapore, 2010.
2 S. V. Aradhya and L. Venkataraman, *Nat. Nanotechnol.*, 2013, **8**, 399–410.
3 J. P. Bergfield and M. A. Ratner, *Phys. Status Solidi B*, 2013, **250**, 2249-2266.
4 M. Paulsson and S. Datta, *Phys. Rev. B: Condens. Matter Mater. Phys.*, 2003, **67**, 241403(R).
5 Y. Dubi and M. Di Ventra, *Rev. Mod. Phys.*, 2011, **83**, 131–155.
6 F. Pauly, J. K. Viljas and J. C. Cuevas, *Phys. Rev. B: Condens. Matter Mater. Phys.*, 2008, **78**, 035315.
7 S. Bilan, L. A. Zotti, F. Pauly and J. C. Cuevas, *Phys. Rev. B: Condens. Matter Mater. Phys.*, 2012, **85**, 205403.
8 C. M. Finch, V. M. García-Suárez and C. J. Lambert, *Phys. Rev. B: Condens. Matter Mater. Phys.*, 2009, **79**, 033405.
9 J. Bergfield, M. Solis and C. Stafford, *ACS Nano*, 2010, **4**, 5314-5320.
10 C. J. Lambert, *Chem. Soc. Rev.*, 2015, **44**, 875-888.
11 N. W. Ashcroft and N. D. Mermin, *Solid State Physics*, Saunders, Philadelphia, PA, 1976.
12 C. Evangeli, M. Matt, L. Rincón-García, F. Pauly, P. Nielaba, G. Rubio-Bollinger, J. C. Cuevas and N. Agraït, *Nano Lett.*, 2015, **15**, 1006-1011.
13 N. Cusack and P. Kendall, *Proc. Phys. Soc.*, 1958, **72**, 898-901.
14 D. M. Rowe, *CRC Handbook of Thermoelectrics*, CRC Press, Boca Raton, FL, 1995.
15 J. P. Heremans, C. M. Thrush, D. T. Morelli and M.-C. Wu, *Phys. Rev. Lett.*, 2002, **88**, 216801.
16 J. Kim, W. Shim and W. Lee, *J. Mater. Chem. C*, 2015, **3**, 11999-12013.
17 S. K. Bux, R. G. Blair, P. K. Gogna, H. Lee, G. Chen, M. S. Dresselhaus, R. B. Kaner and J.-P. Fleurial, *Adv. Funct. Mater.*, 2009, **19**, 2445–2452.
18 T. H. Geballe and G. W. Hull, *Phys. Rev.*, 1954, **94**, 1134-1140.
19 G. Joshi, H. Lee, Y. Lan, X. Wang, G. Zhu, D. Wang, R. W. Gould, D. C. Cuff, M. Y. Tang, M. S. Dresselhaus, G. Chen and Z. Ren, *Nano Lett.*, 2008, **8**, 4670-4674.
20 X. W. Wang, H. Lee, Y. C. Lan, G. H. Zhu, G. Joshi, D. Z. Wang, J. Yang, A. J. Muto, M. Y. Tang, J. Klatsky, S. Song, M. S. Dresselhaus, G. Chen and Z. F. Ren, *Appl. Phys. Lett.*, 2008, **93**, 193121.
21 H. Abrams and R. N. Tauber, *J. Appl. Phys.*, 1969, **40**, 3868-3870.
22 R. Y. Wang, J. P. Feser, X. Gu, K. M. Yu, R. A. Segalman, A. Majumdar, D. J. Milliron and J. J. Urban, *Chem. Mater.*, 2010, **22**, 1943-1945.
23 A. I. Hochbaum, R. Chen, R. D. Delgado, W. Liang, E. C. Garnett, M. Najarian, A. Majumdar and P. Yang, *Nature*, 2008, **451**, 163-167.
24 G. H. Kim, L. Shao, K. Zhang and K. P. Pipe, *Nat. Mater.*, 2013, **12**, 719-723.
25 N. Massonnet, A. Carella, O. Jaudouin, P. Rannou, G. Laval, C. Celle and J.-P. Simonato, *J. Mater. Chem. C*, 2014, **2**, 1278-1283.
26 H. J. Goldsmid, *Introduction to Thermoelectricity*, Springer, Berlin Heidelberg, 2010.
27 J. P. Bergfield and C. A. Stafford, *Nano Lett.*, 2009, **9**, 3072-3076.
28 V. M. García-Suárez, C. J. Lambert, D. Zs. Manrique and T. Wandlowski, *Nanotechnol.*, 2014, **25**, 205402.
29 M. Strange, J. S. Seldenthuis, C. J. O. Verzijl, J. M. Thijssen and G. C. Solomon, *J. Phys. Chem.*, 2015, **142**, 084703.
30 P. Reddy, S.-Y. Jang, R. A. Segalman and A. Majumdar, *Science*, 2007, **315**, 1568-1571.
31 J. R. Widawsky, P. Darancet, J. B. Neaton and L. Venkataraman, *Nano Lett.*, 2012, **12**, 354-358.
32 C. Evangeli, K. Gillemot, E. Leary, M. T. González, G. Rubio-Bollinger, C. J. Lambert and N. Agraït, *Nano Lett.*, 2013, **13**, 2141-2145.
33 T. Morikawa, A. Arima, M. Tsutsui and M. Taniguchi, *Nanoscale*, 2014, **6**, 8235-8241.
34 S. Kaneko, Y. Nakamura, R. Matsushita, S. Marqués-González and M. Kigughi, *Appl. Phys. Express*, 2015, **8**, 065201.
35 Y. Kim, W. Jeong, K. Kim, W. Lee and P. Reddy, *Nat. Nanotechnol.*, 2014, **9**, 881-885.
36 A. Tan, S. Sadat and P. Reddy, *Appl. Phys. Lett.*, 2010, **96**, 013110.
37 W. B. Chang, B. Russ, V. Ho, J. J. Urban and R. A. Segalman, *Phys. Chem. Chem. Phys.*, 2015, **17**, 6207-6211.
38 N. Agraït, J. G. Rodrigo and S. Vieira, *Phys. Rev. B: Condens. Matter Mater. Phys.*, 1993, **47**, 12345-12348.
39 J. M. Krans, C. J. Muller, I. K. Yanson, Th. C. M. Govaert, R. Hesper and J. M. van Ruitenbeek, *Phys. Rev. B: Condens. Matter Mater. Phys.*, 1993, **48**, 14721-14724.
40 J. I. Pascual, J. Méndez, J. Gómez-Herrero, A. M. Baró, N. García and Vu Thien Binh, *Phys. Rev. Lett.*, 1993, **71**, 1852 – 1855.
41 N. Agraït, A. L. Yeyati and J. M. van Ruitenbeek, *Phys. Rep.*, 2003, **377**, 81–279.
42 J. C. Cuevas, A. Levy Yeyati, A. Martín-Rodero, G. Rubio Bollinger, C. Untiedt, and N. Agraït, *Phys. Rev. Lett.*, 1998, **81**, 2990-2993.
43 E. Scheer, N. Agraït, J. C. Cuevas, A. Levy Yeyati, B. Ludoph, A. Martín-Rodero, G. Rubio Bollinger, J. M. van Ruitenbeek, C. Urbina, *Nature*, 1998, **394**, 154-157.
44 A. I. Yanson, G. Rubio Bollinger, H. E. van den Brom, N. Agraït and J. M. van Ruitenbeek, *Nature*, 1998, **395**, 783-785.
45 G. Rubio-Bollinger, S. R. Bahn, N. Agraït, K. W. Jacobsen and S. Vieira, *Phys. Rev. Lett.*, 2001, **87**, 026101.
46 N. Agraït, G. Rubio-Bollinger and S. Vieira, *Phys. Rev. Lett.*, 1995, **74**, 3995-3998.
47 G. Rubio-Bollinger, N. Agraït and S. Vieira, *Phys. Rev. Lett.*, 1996, **76**, 2302-2305.
48 M. A. Reed, C. Zhou, C. J. Muller, T. P. Burgin and J. M. Tour, *Science*, 1997, **278**, 252-254.
49 B. Xu and N. Tao, *Science*, 2003, **301**, 1221–1223.
50 E. Leary, A. La Rosa, M. T. González, G. Rubio-Bollinger, N. Agraït and N. Martín, *Chem Soc. Rev.*, 2015, **44**, 920-942.
51 K. Baheti, J. A. Malen, P. Doak, P. Reddy, S.-Y. Jang, T. D. Tilley, A. Majumdar and R. A. Segalman, *Nano Lett.*, 2008, **8**, 715-719.
52 J. A. Malen, P. Doak, K. Baheti, T. D. Tilley, A. Majumdar and R. A. Segalman, *Nano Lett.*, 2009, **9**, 3406-3412.
53 Y. Dubi, *New J. Phys.*, 2013, **15**, 105004.
54 S. Guo, G. Zhou and N. Tao, *Nano Lett.*, 2013, **13**, 4326-4332.
55 T. Kim, *J. Korean Phys. Soc.*, 2015, **67**, 1553-1557.
56 J. A. Malen, P. Doak, K. Baheti, T. D. Tilley, R. A. Segalman and A. Majumdar, *Nano Lett.*, 2009, **9**, 1164-1169.
57 W. B. Chang, C.-K. Mai, M. Kotiuga, J. B. Neaton, G. C. Bazan and R. A. Segalman, *Chem. Mater.*, 2014, **26**, 7229-7235.
58 D. Kim, P. S. Yoo and T. Kim, *J. Korean Phys. Soc.*, 2015, **66**, 602-606.
59 J. R. Widawsky, W. Chen, H. Vázquez, T. Kim, R. Breslow, M. S. Hybertsen and L. Venkataraman, *Nano Lett.*, 2013, **13**, 2889-2894.

60 E. J. Dell, B. Capozzi, J. Xia, L. Venkataraman and L. M. Campos, *Nat. Chem.*, 2015, **7**, 209-214.
61 S. K. Lee, M. Buerkle, R. Yamada, Y. Asai and H. Tada, *Nanoscale*, 2015, **7**, 20497-20502.
62 L. Rincón-García, A. K. Ismael, C. Evangeli, I. Grace, G. Rubio-Bollinger, K. Porfyrakis, N. Agraït and C. J. Lambert, *Nat. Mater.*, 2015, DOI: 10.1038/NMAT4487.
63 J. A. Malen, S. K. Yee, A. Majumdar and R. A. Segalman, *Chem. Phys. Lett.*, 2010, **491**, 109-122.
64 S. K. Yee, J. A. Malen, A. Majumdar and R. A. Segalman, *Nano Lett.*, 2011, **11**, 4089-4094.
65 S. K. Lee, T. Ohto, R. Yamada and H. Tada, *Nano Lett.*, 2014, **14**, 5276-5280.
66 T. Kim, P. Darancet, J. R. Widawsky, M. Kotiuga, S. Y. Quek, J. B. Neaton and L. Venkataraman, *Nano Lett.*, 2014, **14**, 794-798.
67 J. Vacek, J. Vacek Chocholoušová, I. G. Stará, I. Starý and Y. Dubi, *Nanoscale*, 2015, **7**, 8793-8802.
68 M. Tsutsui, T. Morikawa, Y. He, A. Arima and M. Taniguchi, *Sci. Rep.*, 2015, **5**, 11519.
69 M. Tsutsui, T. Morikawa, A. Arima and M. Taniguchi, *Sci. Rep.*, 2013, **3**, 3326.
70 B. Ludolph and J. M. Van Ruitenbeek, *Phys. Rev. B: Condens. Matter Mater. Phys.*, 1999, **59**, 12290-12293.
71 D. J. Wold and C. D. Frisbie, *J. Am. Chem. Soc.*, 2001, **123**, 5549-5556.
72 A. Tan, J. Balachandran, S. Sadat, V. Gavini, B. D. Dunietz, S.-Y. Jang and P. Reddy, *J. Am. Chem. Soc.*, 2011, **133**, 8838-8841.
73 A. Tan, J. Balachandran, B. D. Dunietz, S.-Y. Jang, V. Gavini and P. Reddy, *Appl. Phys. Lett.*, 2012, **101**, 243107.
74 J. Balachandran, P. Reddy, B. D. Dunietz and V. Gavini, *J. Phys. Chem. Lett.*, 2012, **3**, 1962-1967.
75 J. Balachandran, P. Reddy, B. D. Dunietz and V. Gavini, *J. Phys. Chem. Lett.*, 2013, **4**, 3825-3833.
76 H. S. J. van der Zant, Y.-V. Kervennic, M. Poot, K. O'Neill, Z. de Groot, J. M. Thijssen, H. B. Heersche, N. Stuhr-Hansen, T. Bjørnholm, D. Vanmaekelbergh, C. A. van Walree and L. W. Jenneskens, *Faraday Discuss.*, 2006, **131**, 347-356.
77 Z. M. Wu, M. Steinacher, R. Huber, M. Calame, S. J. Van der Molen and C. Schönenberg, *Appl. Phys. Lett.*, 2007, **91**, 053118.
78 D. V. Talapin, J.-S. Lee, M. V. Kovalenko and E. V. Shevchenko, *Chem. Rev.*, 2010, **110**, 389-458.
79 J. Liao, S. Blok, S. J. van der Molen, S. Diefenbach, A. W. Holleitner, C. Schonenberger, A. Vladyka and M. Calame, *Chem. Soc. Rev.*, 2015, **44**, 999-1014.
80 K.-H. Müller, *J. Chem. Phys.*, 2008, **129**, 044708.
81 F. Pauly, J. K. Viljas, M. Bürkle, M. Dreher, P. Nielaba and J. C. Cuevas, *Phys. Rev. B: Condens. Matter Mater. Phys.*, 2011, **84**, 195420.
82 Z. Wang, J. A. Carter, A. Lagutchev, Y. Kan Koh, N.-H. Seong, D. G. Cahill and D. D. Dlott, *Science*, 2007, **317**, 787-790.
83 M. D. Losego, M. E. Grady, N. R. Sottos, D. G. Cahill and P. V. Braun, *Nat. Mater.*, 2012, **11**, 502-506.
84 T. Meier, F. Menges, P. Nirmalraj, H. Hölscher, H. Riel and B. Gotsmann, *Phys. Rev. Lett.*, 2014, **113**, 060801.
85 S. V. Aradhya, J. S. Meisner, M. Krikorian, S. Ahn, R. Parameswaran, M. L. Steigerwald, C. Nuckolls and Latha Venkataraman, *Nano Lett.*, 2012, **12**, 1643–1647.
86 D. Nozaki, H. Sevinçli, W. Li, R. Gutiérrez, and G. Cuniberti, *Phys. Rev. B: Condens. Matter Mater. Phys.*, 2010, **81**, 235406.
87 E. Zerah-Harush and Y. Dubi, *Phys. Rev. Appl.*, 2015, **3**, 064017.
88 T. Li, J. Rahlf Hauptmann, Z. Wei, S. Petersen, N. Bovet, T. Vosch, J. Nygård, W. Hu, Y. Liu, T. Bjørnholm, K. Nørgaard and B. W. Laursen, *Adv. Mater.*, 2012, **24**, 1333-1339.